GLOBAL BIOGEOCHEMICAL CYCLES, VOL. 13, NO. 1, PAGES 221–250, MARCH 1999

A global oceanic sediment model for long-term climate studies

C. Heinze and E. Maier-Reimer

Max-Planck-Institut für Meteorologie, Hamburg, Germany

A. M. E. Winguth and D. Archer

Department of the Geophysical Sciences, University of Chicago, Chicago, Illinois

Abstract. A chemically reactive 10-layer sediment module was coupled to a geochemical ocean general circulation model (the Hamburg Oceanic Carbon Cycle Model). The sediment model includes four solid sediment components ($CaCO_3$, opal, organic carbon, and clay), and five pore water substances (dissolved inorganic carbon, total alkalinity, PO_4^{3-}, O_2, $Si(OH)_4$) plus corresponding species containing ^{13}C and ^{14}C instead of ^{12}C. The processes, namely, particle deposition, pore water reactions, pore water diffusion and interaction with the open water column, vertical sediment advection, sediment accumulation, and bioturbation, are simulated through basic parametrizations. For the water column part the Si and C cycles are coupled by a formulation of the "rain ratio" Si:C($CaCO_3$):C(POC), where POC is particulate organic carbon, in biogenic particle export production, with $CaCO_3$ frustrule production growing in parallel to a weakening of opal production during progressing deficiency of dissolved silicate in the surface layer. For two preindustrial velocity fields the model reproduces major features of observed water column and sediment tracer distributions parallel to a correct preindustrial CO_2 level close to 280 ppm. The model reacts sensitively to the formulation of the POC flux parametrization, the rain ratio, as well as the solubility of opal but is fairly insensitive to changes in the bioturbation rate as well as the amount of clay deposition. A simulation of the sediment distribution by use of a velocity field, which represents the ocean at conditions during the last glacial maximum, yields realistic glacial-interglacial changes for the Atlantic Ocean, while discrepancies remain for the Indo-Pacific region. A significant decrease of the atmospheric pCO_2 could be achieved through an additional change of water column inventories by a change in weathering input of Si and alkalinity.

1. Introduction

The marine sediment plays a twofold role for climate studies. First it records climatic changes, and second, through its link with the global carbon cycle, it is an active component of the climate system. Sedimentary tracers for climate and the carbon cycle, such as the ^{13}C in shell material from planktonic and benthic foraminifera [e.g., *Shackleton and Pisias,* 1985] but also the concentrations of calcareous and opaline material themselves [e.g., *Keller and Barron,* 1983], provide the foundation for paleoceanography.

Paper number 98GB02812.
0886-6236/99/98GB-02812$12.00

These and other "proxies" and paleoceanographic tracers from the sediment have provided the basis for a validation of modeling efforts in order to understand past climatic fluctuations, also in view of a potential anthropogenically induced climate change. Concerning the active role of the marine sediment within the climate system, the focus has been on $CaCO_3$ sediment and its impact on atmospheric CO_2 through its influence on oceanic alkalinity. Dissolution of $CaCO_3$ sediment can potentially compensate, on a timescale of tens of thousands of years, fossil fuel CO_2 emissions into the atmosphere [*Broecker and Takahashi,* 1977; *Maier-Reimer,* 1989; *Archer et al.,* 1997], though it will not react quickly to large, short-term increases of atmospheric CO_2 concentrations. An increase of oceanic alkalinity linked with an increased corrosion of $CaCO_3$ sediment has also been discussed as one of the causes for the

atmospheric CO_2 drawdown during the last glacial of up to about -100 ppm compared with the preindustrial level of 280 ppm [*Barnola et al.*, 1987; *Staffelbach et al.*, 1991]. Glacial/interglacial changes in $CaCO_3$ sediment may have either been associated with a slowing down of the oceanic circulation and a vertical fractionation of water column tracer concentrations [*Boyle*, 1988] or with changes of the "rain ratio" $C(CaCO_3)$:C(organic C) in the export production of biogenic matter sinking through the water column [*Archer and Maier-Reimer*, 1994].

In model studies both the ability of the sediment to store information and its active role for atmospheric pCO_2 have been investigated. Box models have provided important conceptual insights into potential mechanisms that govern the global oceanic carbon cycle and its link with climatic change [e.g., *Berner et al.*, 1983; *Lasaga et al.*, 1985; *Delaney and Boyle*, 1988; *Munhoven and François*, 1996]. They are lacking, however, from the crude quantification of fluxes and the limited possibility for comparison with actual data which are based on measurements such as variations of the calcium carbonate compensation depth (CCD), the depth where $CaCO_3$ supply from biogenic particle rain balances dissolution. *Heinze et al.* [1991] have used the three-dimensional Hamburg Oceanic Carbon Cycle Model, which is based on the grid and velocity field of an ocean general circulation model (OGCM), in order to identify the cause for the glacial pCO_2 reduction. Owing to the comparatively high resolution of this model, they were able to compare the model results directly with measurements from the sedimentary record. *Archer and Maier-Reimer* [1994] coupled a multilayer $CaCO_3$ sediment model after *Archer* [1991] to the Hamburg Oceanic Carbon Cycle Circulation Model. This study was the first attempt to couple a threedimensional carbon cycle model with a chemically interactive, multilayer sediment module. Their proposed cause for the glacial pCO_2 reduction through an increase in deep water alkalinity parallel to a reduction in $CaCO_3$ production successfully showed similarities to observations from boron isotope analysis [*Sanyal et al.*, 1995].

In this study we extend the former investigative efforts concerning the marine sediment with respect to three issues: (1) The coupling of a chemically interactive, four component sediment model (solid components: $CaCO_3$, organic carbon, opal, and clay) to a geochemical OGCM, (2) the effect of changes in selected water column and sediment parameters on the tracer distributions and atmospheric CO_2, and (3) the sensitivity of the sediment distribution for changes in ocean circulation and the associated impact on atmospheric CO_2.

In the following sections we at first introduce the model and describe the methods for initializing and "tuning" it. After this technical part we present the results of a control run using a velocity field for the preindustrial ocean. Finally, results from sensitivity studies are discussed, which address dilution of the sediment with chemically inert material, the bioturbation rate, the particulate organic carbon (POC) flux through the water column, the rain ratio, the opal solubility, and changes of the velocity field.

2. Model Description

The geochemical OGCM used in this study is based on the geometry, the velocity and thermohaline fields of the dynamical Hamburg Large-Scale Geostrophic Ocean General Circulation Model (LSG-OGCM). In order to find an optimal trade-off between spatial and temporal resolution on one hand and computational economy on the other hand, the 11-layer configuration of *Maier-Reimer et al.* [1993] and *Winguth et al.* [1996] is used here with layer interfaces at 0, 50, 112.5, 200, 350, 575, 850, 1500, 2500, 3500, 4500, and 6000 m. The spatial discretization with an E grid results in a formal horizontal resolution of 3.5°× 3.5°. The geochemical model is an extension of the Hamburg Oceanic Carbon Cycle Circulation Model HAMOCC2 originally developed by *Bacastow and Maier-Reimer* (1990) as well as *Maier-Reimer and Bacastow* (1990). It is used here in the annually averaged version, i.e. with a time step of 1 year, which allows long integration periods of up to several ten thousands of years. The model configuration of *Heinze et al.* (1991) and *Heinze and Maier-Reimer* (1992) has been modified with respect to several issues. The simple interaction of the model water column with "sedimentary pools" which allowed no sediment accumulation, is replaced by a chemically active 10-layer sediment module following the concept of *Archer et al.* [1993]. The Si cycle is implemented and coupled to the carbon cycle through the formulation of the "rain ratio" Si:$C(CaCO_3)$:C(POC) for biogenic particle export production in the model surface layer. The gas exchange formulation for oxygen is replaced by the method applied for CFCs by *Heinze et al.* [1998] and the oxygen cycle is closed allowing for consideration of a global oxygen balance. The implementation of the Si cycle and the closing of the oxygen budget were first carried out by *Maier-Reimer* [1993] and *Six and Maier-Reimer* [1996] in the carbon cycle model version, which uses a time step of 1 month, and hence resolves the seasonal cycle. Processes with time constants shorter than 1 year, such as the O_2 gas exchange across the air water interface and the production of silicate shell material, however, require a modified treatment in the annually averaged version as described below. The effect of the respective processes has to be modeled correctly, while it is, of course, not possible to model details

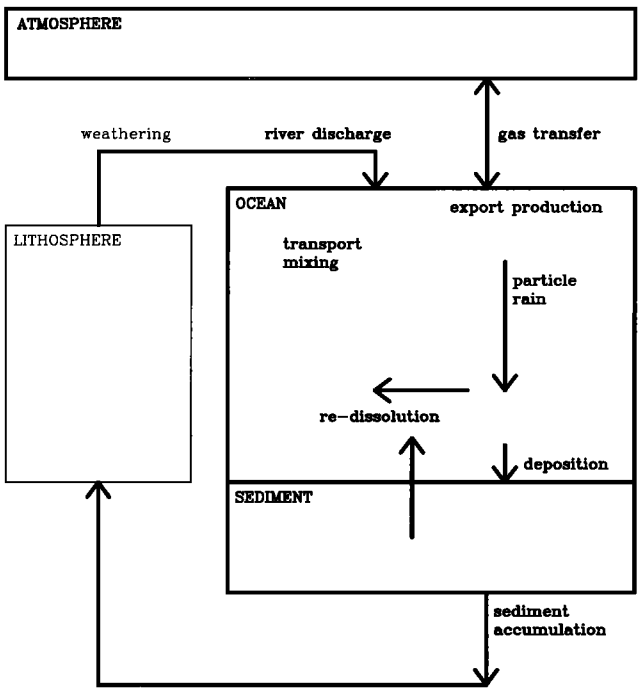

Figure 1. Reservoirs and processes considered by the model. (The lithosphere (thinner lines) is not modelled.)

such as diatom blooms. The seasonally resolving model of *Six and Maier-Reimer* [1996], furthermore, includes a refined trophic model including food web dynamics, especially an explicit prediction of zooplankton, which strongly reduces "nutrient trapping" [see *Najjar et al.*, 1992] in upwelling areas and associated unrealistic O_2 minima.

Basically, the geochemical OGCM is a box model including the reservoirs atmosphere, ocean, and bioturbated sediment, and the associated fluxes between these reservoirs (Figure 1). The processes, namely, diffusive transport in the atmosphere, air/sea gas exchange, biological export production, particle flux through the water column, deposition of material onto the ocean floor, remineralization and redissolution within the water column and the sediment pore waters, transport and mixing in the water column, diffusion of sediment pore waters and interaction with the bottom waters, vertical sediment advection, bioturbation, and sediment accumulation, are parameterized by simple bulk formulas.

Input data for the model are the three-dimensional velocity, convective mixing, sea ice thickness, and thermohaline (potential temperature and salinity) fields from the LSG-OGCM, which had been integrated for 10,000 years into equilibrium, plus fluxes of matter from weathering of terrestrial material. These matter fluxes determine the global sediment accumulation rate of the respective substances in the long-term equilibrium. These weathering fluxes where chosen according to estimates on the basis of observations, which had to be corrected upward for opal later on (see below).

The tracers simulated are, in the atmosphere, $^{12}CO_2$, $^{13}CO_2$, $^{14}CO_2$, and O_2; in the water column, $DI^{12}C$, $DI^{13}C$, $DI^{14}C$, TAlk, PO_4^{3-}, O_2, $Si(OH)_4$, $PO^{12}C$, $PO^{13}C$, $PO^{14}C$; in the sediment pore waters, the same tracers as in the water column except POC, and finally the solid sediment components, $Ca^{12}CO_3$, $Ca^{13}CO_3$, $Ca^{14}CO_3$, $PO^{12}C$, $PO^{13}C$, $PO^{14}C$, opal, and clay (where DIC is total dissolved inorganic carbon, TAlk is total alkalinity, and POC is particulate organic carbon). The tracer transport in the atmosphere and ocean is simulated with the same methods as described by *Maier-Reimer and Hasselmann* [1987] and *Bacastow and Maier-Reimer* [1990], i.e., a diffusive meridional transport within the atmosphere reservoir and an implicit component upstream advection scheme for marine tracer transport. Convective mixing is performed through homogenizing tracer concentrations of two overlying boxes in cases of hydrostatic instability. Complete homogenizing is carried out only if the instability occurs yearround and to a certain percentage if it occurs only during selected months.

2.1. Modeling Strategy

For the control run (C1) the physical input data (velocities, sea ice thickness, convective mixing, potential temperature, and salinity) were taken from the interglacial or preindustrial run "interglacial first guess" (IFG) from *Winguth et al.* [1996]. The forcing fields for this model integration were monthly mean wind stress data taken from an atmospheric circulation model (version 3 of the atmospheric model of the European Center for Medium-Range Weather Forecast, with special modifications for climate studies made by several groups at Hamburg with a truncation of the wave spectrum at wavenumber 42 or the so called ECHAM3/T42) [*Lorenz et al.*, 1996], monthly averaged air temperatures from the Comprehensive Ocean Atmosphere Data Set (COADS) [*Woodruff et al.*, 1987], and climatological annually averaged surface salinities after *Levitus* [1982]. Details concerning the physical LSG-OGCM integration are described by *Winguth et al.* [1996].

Directly comparable to this control run velocity field, a glacial ocean velocity field is available, which was used in a sensitivity study. This velocity field was also provided by *Winguth et al.* [1996] ("glacial first guess" (GFG)). It was obtained by use of prescribed 2-m air temperatures and wind stresses from a glacial Atmospheric General Circulation Model (AGCM) simulation with the ECHAM3/T42 model [*Lorenz et al.*, 1996]. Wind stress data from the corresponding preindustrial AGCM run were already taken as input for the control run velocity field. The glacial velocity field was produced by *Winguth et al.* [1996] in order to get as close

as possible to a realistic glacial ocean circulation for further assimilation of sediment core $\delta^{13}C$ data. The freshwater flux forcing for the dynamical ocean model was modified to glacial conditions on the basis of surface salinity reconstructions for the last glacial maximum [*Duplessy et al.*, 1991, 1996] plus additional corrections as described by *Winguth et al.* [1996].

In order to enable comparison with former carbon cycle model runs, an additional preindustrial model run was carried out with the velocity field which already was used by *Heinze et al.* [1991] and (coupled to the sediment model) by *Heinze and Crowley* [1997]. This velocity field ("ATOS1" annually averaged, from [*Maier-Reimer et al.*, 1993]) differs from the velocity field of *Winguth et al.* [1996] as used for our control run here with respect to the atmospheric forcing and the bottom topography (northern rim of Greenland). Instead of wind stress data as derived from an atmospheric general circulation model, in the work of *Maier-Reimer et al.* [1993], climatological data based on observations [*Hellerman and Rosenstein*, 1983] were used. Both preindustrial velocity fields, however, employ the same general vertical and horizontal grid geometry.

2.2. The Inorganic Carbon Cycle

The inorganic carbon cycle system is modeled following *Maier-Reimer and Hasselmann* [1987] and *Heinze et al.* [1991] including the two dissociation steps of carbon acid and the borate buffer system. The dissociation constants for carbonic acid K_1, K_2, the dissociation constant for boric acid K_B, and the ionic product of water K_W were computed according to *Roy et al.*, [1993], *Edmond and Gieskes*, [1970], and *Dickson and Riley*, [1979] (coefficient for salinity dependency of K_W corrected from 0.9415 to 0.09415) respectively. Pressure correction was applied after *Culberson and Pytkowicz*, [1968]. The $[H^+]$ is computed from insertion of DIC into TAlk [*Maier-Reimer and Hasselmann*, 1987, equation (20)] by use of a one-dimensional Newton-Raphson algorithm.

2.3. Gas Exchange Between Ocean and Atmosphere

Air/sea gas exchange for CO_2 is performed in the same manner as in the work by *Heinze et al.* [1991]. The equilibration time for oxygen in oceanic surface waters is about 10 times faster than that for CO_2 because no buffer factor applies for oxygen. In order to appropriately account for this short equilibration time in the annually averaged model version, the formulation of *Heinze et al.* [1998] which was used for simulation of the CFC source function, was applied for oxygen. The concentration change of oxygen in the model surface layer due to gas exchange is

$$\frac{dC}{dt} = F/\Delta z, \tag{1}$$

where C is oxygen concentration, F is O_2 flux across the water/air interface, and Δz is the surface layer thickness.

The numerical scheme for the oceanic O_2 concentration is then, according to the analytical solution of (1),

$$C^{\text{new}} = C_{\text{equilibrium}} + (C^{\text{old}} - C_{\text{equilibrium}})e^{(-k_{av}/\Delta z)\Delta t} \tag{2}$$

where

C^{new} oceanic concentration at the new time step;
C^{old} oceanic concentration at the previous time step;
$C_{\text{equilibrium}}$ oceanic concentration for solubility equilibrium with atmosphere;
k_{av} gas transfer velocity;
Δz depth of the layer which exchanges directly with atmosphere;
Δt time step (here, 1 year).

Oxygen concentrations are thus set to the solubility equilibrium value for the surface layer, except in regions of convective overturning, where the flux of oxygen into the ocean is distributed over the entire unstable water column (instead of Δz = the surface layer thickness only in the stable case). Measurements indicate a gas transfer velocity for oxygen of about 1000 to 2000 m/yr [*Broecker and Peng*, 1982]. In the model, however, for k_{av}, a constant value of 250 m/yr was set. This leads only to a negligible error in stably stratified water but accounts for the fact that in active deep water production areas, the contact of overturning water is too short to allow achievement of full solubility equilibrium between the oceanic surface layer and the atmosphere. A sensitivity experiment with a value of k_{av}=2500 m/yr, indeed, resulted in a realistic O_2 inventory in the upper 500 m but in too high deep water oxygen levels. The oxygen production due to primary production of organic matter is computed from the modeled POC production through a Redfield ratio of C:ΔO_2 of 122:172 [*Takahashi et al.*, 1985]. The revised O_2 exchange formulation leads to an effective deep-sea oxygen ventilation mechanism for the 1-year time step model and an improvement of modeled O_2 water column distributions as compared to earlier model versions [e.g., *Heinze*, 1990].

2.4. Biogenic Particle Export Production

Four different kinds of particles are included in the model: POC, $CaCO_3$, opal, and clay (a terrestrial, nonbiogenic, chemically inert mineral phase, mainly the weathering product of continental crust). The production of biogenic matter is assumed to be limited by nutrient supply and physical growth conditions (such as light, temperature, turbulence, sea ice cover, etc.). We

assume that for POC production, the biolimiting substance is dissolved phosphate, and for opal growth, it is silicic acid.

In the seasonally resolving version of the geochemical model (time step of 1 month), the production of biogenic $CaCO_3$ and opal hard part production is computed on the basis of the monthly POC production [*Maier-Reimer,* 1993]. In order to allow time constants for nutrient uptake that are shorter than 1 year, in the annually averaged model, an alternative formulation for the production rates and hence the rain ratio Si:C($CaCO_3$):C(POC), has to be provided. POC as well as opal production are computed implicitly within the advection algorithm (as for POC export production by [*Heinze et al.,* 1991]), where the nutrient uptake follows Michaelis-Menten kinetics [e.g., *Parsons and Takahashi,* 1973]:

$$P_{\mathrm{POC}} = a\left(\frac{V_{\max}^{\mathrm{POC}}[PO_4^{3-}]^2}{K_s^{\mathrm{POC}}+[PO_4^{3-}]}\right) \quad (3)$$

$$P_{\mathrm{opal}} = a\left(\frac{V_{\max}^{\mathrm{opal}}[Si(OH)_4]^2}{K_s^{\mathrm{opal}}+[Si(OH)_4]}\right) \quad (4)$$

where

P_{POC} POC production;
a parameter for physical growth conditions;
$V_{\max}^{\mathrm{POC}}$ maximum uptake rate of phosphate;
K_s^{POC} half saturation constant for POC production;
P_{opal} opal production;
$V_{\max}^{\mathrm{opal}}$ maximum uptake rate of silicate;
K_s^{opal} half saturation constant for opal production.

For the uptake rates and half saturation constants, values of $V_{\max}^{\mathrm{POC}} = 1\ \mathrm{yr}^{-1}$, $K_s^{\mathrm{POC}} = 8.2\times10^{-8}$ mol/L, $V_{\max}^{\mathrm{opal}} = 2.5\ \mathrm{yr}^{-1}$, $K_s^{\mathrm{opal}} = 8.2\times10^{-9}$ mol/L were used. The favoring of Si uptake compared to P uptake was derived from the faster reduction of silicic acid during phytoplankton growth [*Chipman et al.,* 1993]. Values of $[a\ V_{\max}^{\mathrm{POC}}]$ follow the annually integrated light supply function as used in the control experiment of *Heinze et al.* [1991]. $CaCO_3$ production is computed according to the resulting ratio of opal to POC production rate. In cases where this ratio sinks to a given threshold value, production of $CaCO_3$ parallel to opal material is allowed, with increasing $CaCO_3$ percentages as the supply of silicic acid sinks:

$$P_{\mathrm{CaCO3}} = P_{\mathrm{POC}}\, r\, (1-\frac{P_{\mathrm{opal}}}{P_{\mathrm{POC}}}/S_{\mathrm{opal}})\,; \quad \frac{P_{\mathrm{opal}}}{P_{\mathrm{POC}}} < S_{\mathrm{opal}} \quad (5)$$

with P_{CaCO3} the $CaCO_3$ production and the tunable constants r as well as the threshold value S_{opal}. Here r is the parameter for determining the rain ratio C($CaCO_3$): C(organic C) in the absence of any dissolved silica, i.e. the maximum possible fraction of $CaCO_3$ material that can be produced. Measurements of coccolithophorid and diatom abundancies and also sediment trap data indicate a preferential production of opaline shell material in highly productive zones and a reduction of $CaCO_3$ flux relative to POC flux in Southern Ocean water [*Dymond and Lyle,* 1985]. High production zones as well as the Antarctic ocean are upwelling areas where nutrients are brought to the surface. With given evidence for a higher uptake rate of Si than of PO_4^{3-} we conclude that in those regions, preferentially opaline hard part material is produced, owing to availability of silicic acid within the euphotic zone. All biogenic production rates are export production figures. Gross production rates are irrelevant for the annual net CO_2 flux between ocean and atmosphere.

The particles that have been produced through consumption of nutrients and carbon in the model surface layer are redistributed in the water column in order to parameterize the particulate flux. Opal and $CaCO_3$ fractions, which according to this formulation are suspended within the water column, are redissolved within one time step, while POC is remineralized, as long as dissolved O_2 is available, with a time constant of 0.05 per year. Thus the model carries suspended POC but no suspended floating $CaCO_3$ and opal particles, in agreement with observational evidence. POC is redistributed with an exponential profile of e-folding depth 770 m (that is, in 770 m depth, the vertical flux rate of POC is reduced to $1/e$ of the export production rate), following *Volk and Hoffert* [1985] and *Najjar et al.* [1992], whereas for $CaCO_3$ and opal, e-folding depths of 2 and 10 km are used, respectively, which is in rough agreement with sediment trap findings [*Honjo et al.,* 1982]. The portion of the particles that does not get stuck in the water column forms the upper boundary condition of the sediment model and is deposited onto the model ocean floor, i.e., enters directly the uppermost sediment layer. The shallower the model bottom is at a respective grid point, the higher the particle deposition normalized to the export production is and the more it is shifted toward POC deposition owing to the different flux profiles for the different particle species. As a terrestrial component a globally constant "clay " flux of 0.25×10^{-8} mol/(cm^2/yr) was set, assuming that clay has the composition of illite. This is a crude assumption that has to be refined in future model versions. The value for this flux was chosen in order to achieve reasonable bulk accumulation rates in oligotrophic regions such as the North Pacific.

2.5. Sediment-Pore Water Chemistry and Sediment Accumulation

Under each wet ocean grid point of the model a 10-layer sediment model is implemented. The model conceptually follows the approach of *Archer et al.* [1993].

It differs from this model with respect to the numerical formulation, the boundary conditions, and the additional implementation of ^{13}C and ^{14}C in all pore water and solid substances containing carbon. The sediment model is restricted to the upper 10 cm of sediment. It is assumed that this is the major part of the bioturbated sediment mixed layer. Below 10 cm depth within the sediment, any material is considered as "diagenetically consolidated" and is not anymore chemically interacting with pore waters. This procedure is based on measured sediment pore water profiles which indicate an asymptotic approach to a constant concentration in several centimeters depth of the sediment [e.g., *Archer et al.*, 1989, 1993; *Hales and Emerson,* 1996; *Van Bennekom,* 1996]. The vertical resolution decreases with depth in the sediment. Model sediment layer interfaces are defined at 0, 0.3, 0.6, 1.1, 1.6, 2.1, 3.1, 4.1, 5.1, 7.55, and 10.0 cm, while porosities (fraction of pore water volume with respect to total sediment volume) decrease from 0.95 to 0.75, following obervations from *Ullman and Aller* [1982].

The sediment model is based on the equilibrium sediment accumulation = deposition − redissolution, as in the work of *Archer et al.* (1993). The basic equations for solid sediment components S and concentrations of dissolved substances P within the pore water are

$$\frac{dS}{dt} = D_B \frac{\partial^2 S}{\partial z^2} - \frac{\partial}{\partial z}(w\,S) - \frac{R\,M}{\rho\,(1-\Phi)} \quad (6)$$

$$\frac{dP}{dt} = \frac{\partial}{\partial z}(D_W \frac{\partial P}{\partial z}) + \frac{R}{\Phi} \quad (7)$$

where

S solid component (in weight fraction of total sediment);
P dissolved pore water component ;
D_B diffusion coefficient for bioturbation;
w vertical advection velocity of solid compounds;
R reaction rate ;
M molecular weight of solid component ;
ρ density of bulk sediment ;
Φ porosity ;
D_W diffusion coefficient for pore water diffusion.

Of major interest in our studies is the interaction between sediment and open water column. The water column concentrations are not taken as upper fixed boundary conditions for pore water diffusion as in most of the one-dimensional sediment models. Rather, the lowest wet water column box was included in the pore water diffusion of (7), under the assumption that the water column tracer concentration of the bottom water box is reached 1 cm above the sediment water interface and that the bottom water box is well mixed. No explicit computation of the matter flux across the sediment water boundary was used (no linear approximation of the concentration gradient and a corresponding effective sublayer thickness δ_e=1 mm as described by *Boudreau* [1997], which explains our choice of a larger "nonlinear" diffusive sublayer thickness). Few in situ measurements of the diffusive sublayer thickness are available. These indicate values of 0.5 to 3.5 mm in the deep Santa Catalina Basin [*Archer et al.,* 1989]. The potential overestimate of the diffusive sublayer thickness in the model was tested in a run where a value of 1 mm instead of 1 cm was used. The resulting changes after 20,000 years integration time were negligibly small. For the calculation of the reaction rates, uniform kinetics are used. In cases of undersaturation of the pore waters with respect to $CaCO_3$ and opal, the maximum dissolvable amount (difference between pore water saturation value and actual pore water concentration resulting from the previous time step) is brought into solution within one sediment model time step (1/50 year). Respectively, POC within the sediment is remineralized corresponding to the actual dissolved oxygen pore water concentration. No anaerobic organic matter degradation is included. Differential kinetics are discussed and tested in laboratory experiments. Findings from these experiments may not be easily transferable to the real world as discussed by *Keir* [1980] for $CaCO_3$. Opal solubility is influenced by a series of complex processes and, up until now, neither rigourously quantifiable nor even understood [*Hurd,* 1972; *Raguenau et al.,* 1996]. Dissolution kinetics for opal may vary by several orders of magnitude due to inhibition of dissolution in cases of Al contamination [e.g., *Van Bennekom et al.,* 1991]. In our study an opal saturation value of 1000 μmol/L was set for $Si(OH)_4$. Using a single saturation value and linear dissolution kinetics for opal leads to a too high sensitivity of the sedimentary opal distribution from the opal rain rate [*Archer et al.,* 1993]. For sediments in the Indian Ocean sector of the Southern Ocean, flow-through-experiments in the laboratory have substantiated the influence of Al on opal solubility and further suggest a nonlinear dissolution kinetics formulation with exponentially increasing dissolution rates with degree of undersaturation [*Van Capellen and Qiu,* 1997a, b]. Once the underlying mechanisms have been identified on the basis of field studies, the treatment of dissolution kinetics will be be improved in future studies including refinement of the organic carbon budget.

For all dissolved species a uniform pore water diffusion coefficient of $8\times10^{-6}cm^2/s$ multiplied by the respective porosity is used. Experimentally derived diffusion coefficients do not deviate much from this value [*Li and Gregory,* 1974; *Ullman and Aller,* 1982]. At each grid point, pore water diffusion is simulated by an implicit numerical scheme, taking into account the variable grid point spacing, the variable porosities, and decreasing diffusion coefficients with decreasing porosity.

Owing to the redissolution and remineralization of solid matter within the bioturbated sediment mixed layer, gaps in the volume of solid materials are produced. It is assumed that these gaps are filled with solid material again subsequently. On the other hand, new material is deposited onto the uppermost sediment layer, leading to an additional amount of solid matter. The concept is that the geometry of the sediment layers remains the same, i.e., that the layer volumes and porosities remain fixed. Therefore the gaps within the sediment have to be filled again with solid material, and additional material has to be transported downward by a vertical shift of the entire local sediment column relative to the given sediment geometry. Within this context, three different cases have to be considered (see Figure 2).

(1) The deposition onto the uppermost sediment layer is higher than the redissolution and remineralization rate of the entire sediment column. In this case, solid material is accumulated, which means that it leaves the bioturbated zone and disappears into the "diagenetically consolidated" material; that is, sediment accumulation takes place.

(2) No particle deposition takes place (e.g., because of a change in the velocity field and a shift of sea ice cover), but redissolution of previously deposited material goes on. In this case, no sediment accumulation occurs. The gaps within the sediment are closed by filling of material from below. With respect to the bottom layer of the bioturbated sediment, only chemically inert material is used for filling up the sediment. In case of continuing redissolution, finally, only clay would exist at the respective grid point. In reality, also, reactive material could be mixed upward again. Here we did not consider this process, as a detailed global downcore database would be necessary to accomplish this and the amount of reactive material, which is potentially available until lower sediment layers are sealed off from further reaction by refractory material, is difficult to quantify.

(3) Particle deposition is greater than the redissolution of the uppermost sediment layer but smaller than the redissolution from the entire sediment column. Sediment advection changes its direction somewhere within the bioturbated zone. No accumulation occurs.

Bioturbation is parameterized as a diffusion of solid components with closed boundaries at the sediment/bottom water interface and the lower boundary of the bioturbated sediment zone in 10 cm depth. The same basic scheme as for the pore water diffusion is carried out for bioturbation. To some degree, an implicit mixing of

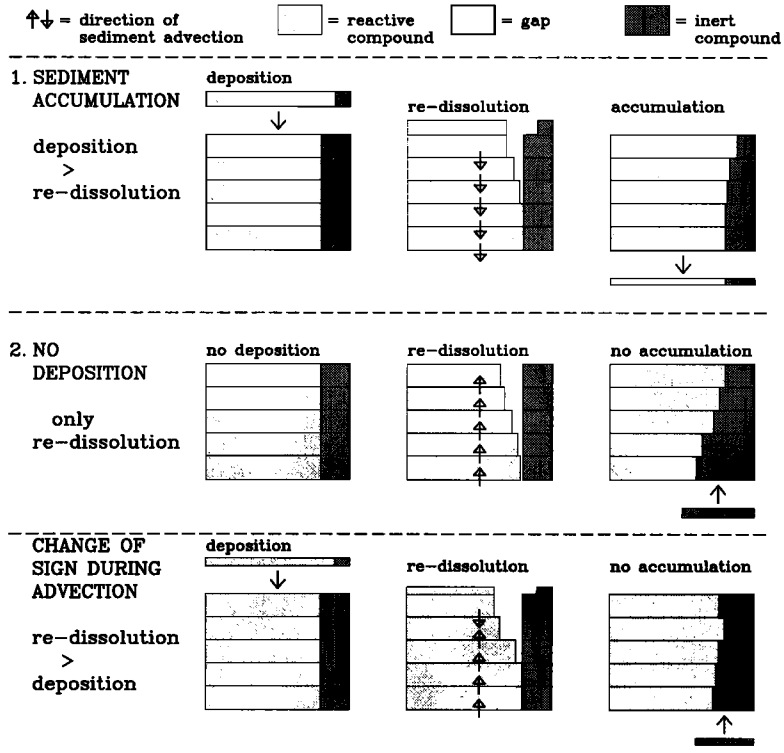

Figure 2. Schematic of the three cases for vertical sediment advection and sediment accumulation. (1) Sediment accumulation takes place. (2) No deposition. (3) Change of advection direction within the bioturbated zone. Here only two different solid compounds (one chemically reactive and one inert component) and five layers are shown for simplicity.

the solid sediment components occurs owing to the sediment advection and accumulation scheme. Therefore an explicit diffusion coefficient of 15 $cm^2/(1000$ years) is set here, which is at the lower margin of the values derived from measurements [cf. *Soetaert et al.*, 1996].

Initial values for the sediment pore water concentrations are set to the respective values of the locally overlying bottom waters for $DI^{12}C$, $DI^{13}C$, $DI^{13}C$, TAlk, O_2, PO_4^{3-}, and $Si(OH)_4$. Solid sediment initial condition is chemically inert clay sediment everywhere, so that the model builds up completely its own biogenic sediment. The water column concentrations themselves are initialized on the basis of a preliminary former carbon cycle model run. In order to start from a status with reasonable oceanic matter inventories for the water column properties, the model inventories were adjusted layerwise to observed data. For this purpose, the mean deviation of the model from observed data (of the Geochemical Ocean Sections Study (GEOSECS)) was determined. Subsequently, the model concentrations were adjusted, so that at the beginning of the integration the model water mass property inventories were in full agreement with the observations. If the mean model profiles of the water column concentrations deviated considerably from the mean observed profiles already within a short integration period, the corresponding model parameter set was rejected and a new attempt was started. Besides the water column profiles, the atmospheric CO_2 partial pressure is used as an indicator for an acceptable simulation. For preindustrial simulations we aimed at achieving a value close to the level of 280 ppm as documented from ice core analysis [*Neftel et al.*, 1985; *Friedli et al.*, 1986]. The weathering rates and thus implicitly the globally integrated sediment accumulation rates for the model were chosen on the basis of estimates from the literature. The weathering fluxes are added as a constant increment to each wet grid point surface ocean box. A future refinement of the input through terrestrial weathering (regionally varying, only along the coastlines for river discharges, according to model predictions for oceanic dust input from the atmosphere) could potentially improve the results, at least locally. The model parameters as used for the reference run including the weathering rates are summarized in Table 1.

In the former model configuration without sediment accumulation [e.g., *Heinze et al.*, 1991], tuning of the model with respect to the atmospheric CO_2 could be easily carried out by slightly adjusting the inventories of TAlk and DIC in the water column. With the actual model, this method does not work anymore, because the balance between sediment and water column may shift after an adjustment of these inventories and compensate for it or even counteract it in the final result. Therefore the rain ratio, primarily the threshold value for the start of $CaCO_3$ production, is used for fine-tuning the model's atmospheric pCO_2. Alternatively, the material input rates through weathering could be used for this tuning. The long time constant for adjustment to changes in weathering fluxes, however, would

Table 1. Overview for Tunable Model Parameters of the Geochemical Model and Respective Values as Used in the Control Run

Tunable Parameter	Value as Set for Control Run
Growth conditions for plankton a (equation (3))	light profile after *Bacastow and Maier-Reimer* [1990] and *Heinze et al.* [1991]
Vertical particle flux profile for POC	exponential profile with e-folding depth of 770 m [*Volk and Hoffert*, 1985]
Verticle particle flux profile for $CaCO_3$	exponential profile with e-folding depth of 2000 m
Vertical particle flux profile for opal	exponential profile with e-folding depth of 10,000 m
Lower threshold value for start of $CaCO_3$ production S_{opal} (equation (5))	0.35506
Parameter r for increase of $CaCO_3$ shell growth (equation (5))	0.5
Maximum uptake rate of phosphate V_{max}^{POC}	1 yr^{-1}
Half saturation constant for POC growth K_s^{POC}	8.2×10^{-8} mol/L
Maximum uptake rate of silicate V_{max}^{opal}	2.5 yr^{-1}
Half saturation constant for opal shell growth K_s^{opal}	8.2×10^{-9} mol/L
Terrestrial clay input	0.25×10^{-8} mol/(cm^2 yr)
Global weathering input of opal	14.9 Tmol/(10^3 yr)
Global weathering input of $CaCO_3$	14.9 Tmol/(10^3 yr)
Global weathering input of POC	5 Tmol/(10^3 yr)
Time constant for POC remineralization	0.05 yr^{-1}
Saturation concentration of pore water $Si(OH)_4$	1000 μmol/L

Table 2. Results of Control Run and Sensitivity Experiments

Experiment	Experiment Description	pCO_2 ppm	POC production GtC/yr	$CaCO_3$ production GtC/yr	opal production 10^{15}mol/yr
–	observation	270-280[a]	3.4[b]–21.9[c]	(0.85-5.5)[d]	(< 0.2-0.28)[e]
C1	control run	278	8.9	1.8	0.17
S1	clay input x 100	278	8.9	1.7	0.17
S2	bioturbation x 0.1	279	8.9	1.8	0.17
S3	bioturbation x 10	279	8.9	1.8	0.17
S4	POC profile after *Martin et al.* [1987]	296	8.2	1.6	0.17
S5[f]	POC profile after *Suess* [1980]	971	16.7	5.5	0.17
S6	threshold value S_{opal} for onset of $CaCO_3$ production minus 10%	255	8.9	1.5	0.17
S7	pore water $Si(OH)_4$ saturation × 2	177	8.9	1.0	0.27
S8	pore water $Si(OH)_4$ saturation × 0.5	414	8.9	2.6	0.11
C2	second preindustrial run, velocities after *Maier-Reimer et al.* [1993]	283	8.8	2.0	0.17
G1	last glacial maximum velocities	312	9.9	2.3	0.15
G2	last glacial maximum velocities plus 50% increase of $Si(OH)_4$ and CO_3^{2-} input through weathering	218	10.0	1.97	0.18

[a]Value is from *Neftel et al.* [1985] and *Friedli et al.* [1986].
[b]Range is 3.4-4.7 GtC/yr after *Eppley and Peterson* [1979].
[c]Value is from *Packard et al.* [1988].
[d]Corresponding to 25% of POC production; an estimate after *Broecker and Peng* [1982].
[e]Value is for total production rate [*Nelson et al.*, 1995]; export production rate would be lower.
[f]Integration was stopped after 6390 years.

involve very long integration periods during the tuning process. Before discussing the result, the model has to be integrated at least for about 20,000 years in order to adjust the sediment distribution. Not only the ocean water column but also the global bioturbated sediment has to be "flushed" once at least. A reliable indicator for the model to be in equilibrium and mass conserving is the resulting pCO_2 time rate of change in the atmosphere reservoir (0.0025 ppm per 1000 years integration time at the end of the control experiment).

3. Control Run Results

For the control run (C1), tunable parameters were adjusted to the values given in Table 1. The model was integrated for 50,000 years after the last, small, modification of the code. During this time the resulting atmospheric pCO_2 already was at steady state with negligible fluctuations. Results for the export production rates as well as the atmospheric CO_2 concentration are close to estimates based on observations (Table 2). The parameters controlling the production of $CaCO_3$ shell material (equation (5)) were set to r=0.5 and S_{opal}=0.35506 in the control experiment. (The five digits for this parameter result from fine-tuning of the model in order to match exactly the preindustrial CO_2 partial pressure; the senstivity of this parameter is tested in an experiment below.) This means that in the model, at molar production ratios of Si/C(POC) higher than about 0.35, no $CaCO_3$ shell material is produced. This value is in a realistic range in view of measurements of Si/C in living diatoms as well as suspended particulate bulk material in surface waters (see discussion by *Nelson et al.* [1995]), indicating higher values than this only in the Southern Ocean and nutrient rich river plumes.

The structure of tracer distributions in the water column is comparable to the results of *Maier-Reimer* [1993]. Mean profiles of modeled and observed tracers from the GEOSECS program are given in Figure 3. For the model profiles in Figure 3, only those grid points were used where respective measurements from GEOSECS were available. While the agreement between observed and modeled DIC, PO_4^{3-}, O_2 is excellent, discrepancies remain for TAlk, dissolved $Si(OH)_4$, and $\Delta^{14}C$. Surface TAlk values indicate that the overall $CaCO_3$ production may be overestimated in the present model, though the global export production rain ratio C($CaCO_3$):C(POC)= 0.2 coincides nicely with independent estimates [*Broecker and Peng*, 1982]. The curvature of the mean TAlk profile as simulated differs from

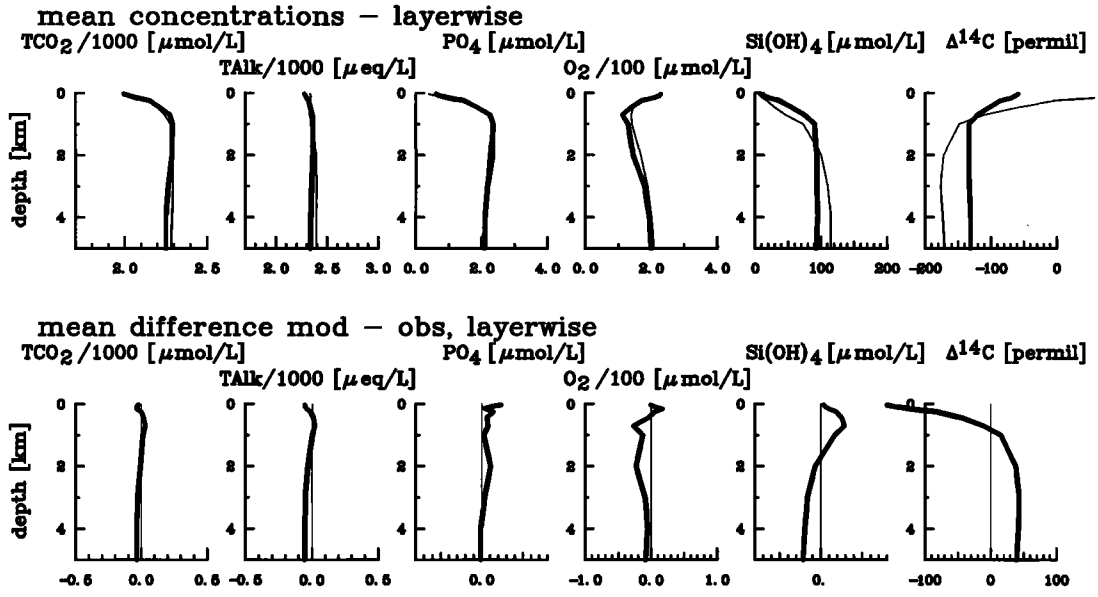

Figure 3. Comparison of the modeled (thick lines) and observed (thin lines, Geochemical Ocean Sections Study (GEOSECS) data) geochemical inventories for the control run by use of the preindustrial oceanic velocity field from *Winguth et al.* [1996]. (top) Mean profiles and (bottom) mean deviations between model and observations.

the observed profile in the upper 1 km of the water column, indicating that the $CaCO_3$ flux parameterization with the exponential profile as chosen for the control run could be refined by regionally differing flux profiles. The large difference between observed and modeled radiocarbon in the upper and intermediate waters is due to the lack of bomb ^{14}C in the preindustrial simulation and hence is not a serious point to worry about. The too young deep water is, in part, a consequence of the low vertical resolution (compare with the 15-layer version of *Maier-Reimer* [1993], showing improved deep water ages compared to the 11-layer model as used in this study). The differences in deep ^{14}C and silicic acid concentration between simulation and actual data from the real world show similar behavior, indicating that both, the errors in $Si(OH)_4$ and radiocarbon may be due to the same reason. As radiocarbon depends primarily on abiotic factors, i.e., the velocity field, the atmospheric source, and in situ radio decay, and not on biological processes such as biogenic matter production and remineralization, the remaining discrepancies can be caused by deficiencies of the model velocity field. *Broecker et al.* [1995] pointed out the high correlation of $Si(OH)_4$ and $\Delta^{14}C$ in the water column below the main thermocline and away from large deep water production areas. This high coupling between the two tracers may apply also for the simulated distributions. In any case it seems to be possible to arrive at well simulated nutrient distributions (here, PO_4^{3-}) even if the radiocarbon distribution is not perfect. This indicates that part of the model deficiencies due to errors in the velocity field can be compensated by biogeochemical model parameters.

The POC export production pattern of the new model run is close to earlier simulations [*Heinze,* 1990] and hence not shown here. The horizontal distributions of the simulated rain ratios $C(CaCO_3)$:C(POC) and Si(opal):C(POC) show how the model discriminates between the different biogenic particle species (Figures 4 and 5). In upwelling regimes, regions of convective overturning, and close to the ice edge, where comparatively high nutrient amounts are available, preferentially opal frustrules are produced (eastern equatorial Pacific, Southern Ocean, western North Pacific, western North Atlantic). In oligotrophic regions and zones of moderate availability of nutrients, $CaCO_3$ shell production dominates (central and western equatorial Pacific, midgyre regions of the subtropical gyres in the northern and southern Atlantic and Pacific). This behavior is in qualitative agreement with the findings from observations [*Dymond and Lyle,* 1985]. Also, quantitatively, the modeled rain ratio values are within the range given by observations in the field and the laboratory [*Brzezinski,* 1985; *Nelson et al.,* 1995]. A temperature correction as applied for $CaCO_3$ production in the earlier model [see *Heinze et al.,* 1991] has proven to be ineffective and is now omitted. The formulation as used here automatically leads to high opal production rates in the Southern Ocean and hence diminished $CaCO_3$ production.

The sediment distributions (vertical averages over all 10 layers of bioturbated sediment) show the ability of the model to reproduce major features of the observed large scale sediment distribution (Figures 6 and 7), namely, $CaCO_3$ sediments prevailing throughout the

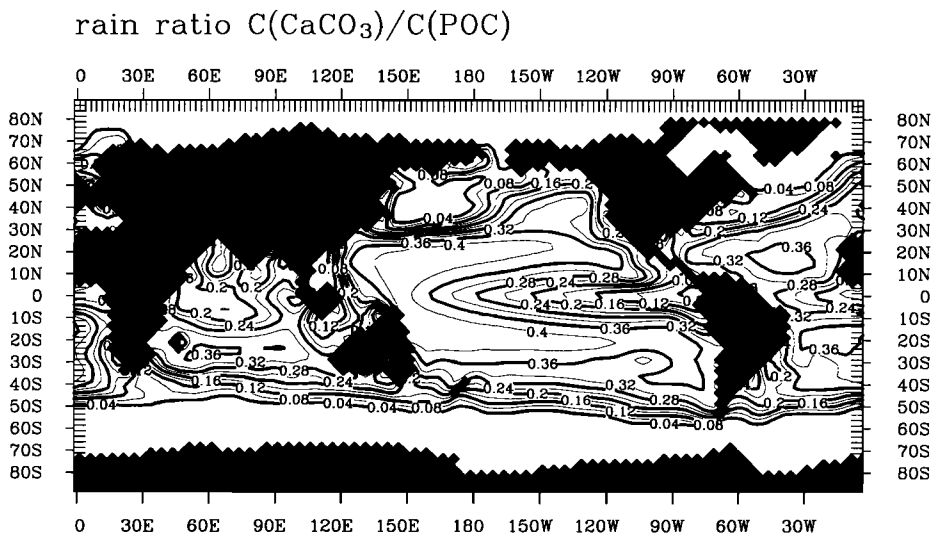

Figure 4. Rain ratio $C(CaCO_3)$:C(POC) of biogenic export production for the control experiment.

Atlantic Ocean as well as in the central Pacific and Indian Oceans and opaline belts in the Southern Ocean and the eastern equatorial Pacific. The $CaCO_3$ distribution pattern compares well with the synoptic global distribution as given by *Archer* [1996, Figure 13, p. 172]. Quantitatively, however, the model overestimates the percentage of $CaCO_3$ in calcareous sediments by about a factor of 1.2 probably in part due to the crude parametrization of terrestrial detrital material fluxes. A closer view of the comparison with observed data (see [*Archer,* 1996], http://popeye.uchicago.edu/) reveals a too high percentage of $CaCO_3$ in the western part of the Atlantic (Figure 8). The reason for this model deficiency is probably a general overestimation of export production in this area due to an unsatisfactory representation of shelf systems in combination with the local Ekman divergence.

In the eastern equatorial Pacific, opal sediment concentrations are clearly too high as compared with observed values (see Figure 9, observed data from the compilation of D. Archer, http://popeye.uchicago.edu/, this data is mainly based on *Lisitzin* [1971] *Lisitsyn* [1986a, b, c], *Leinen et al.* [1986], and *Lyle et al.* [1988]). Though there is significant opal deposition in today's ocean in this region, not much opal is actually accumulated [*DeMaster,* 1981]. The opal production, deposition, and accumulation in the model is too strong due to "nutrient trapping" in the eastern equatorial ocean, a feature of particle-only models [*Najjar et al.*, 1992], which could be removed by use of

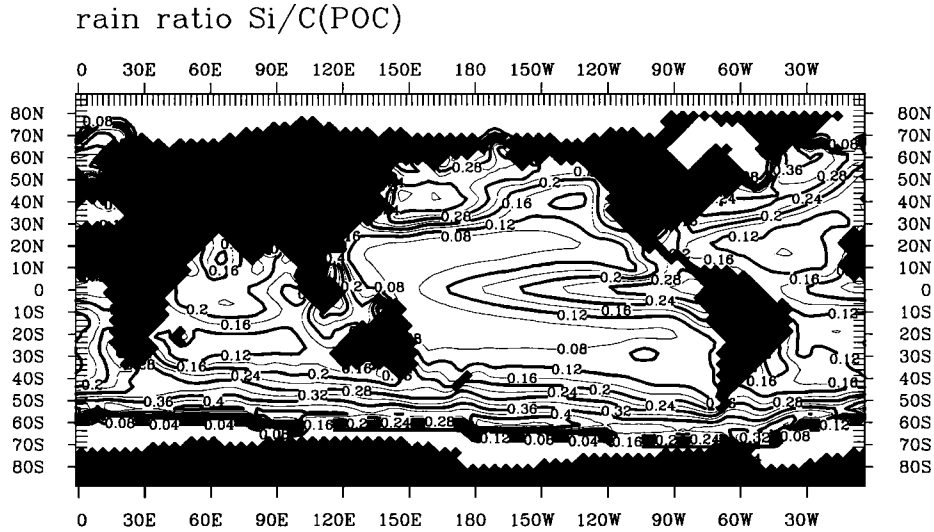

Figure 5. Rain ratio Si(opal):C(POC) of biogenic export production for the control experiment.

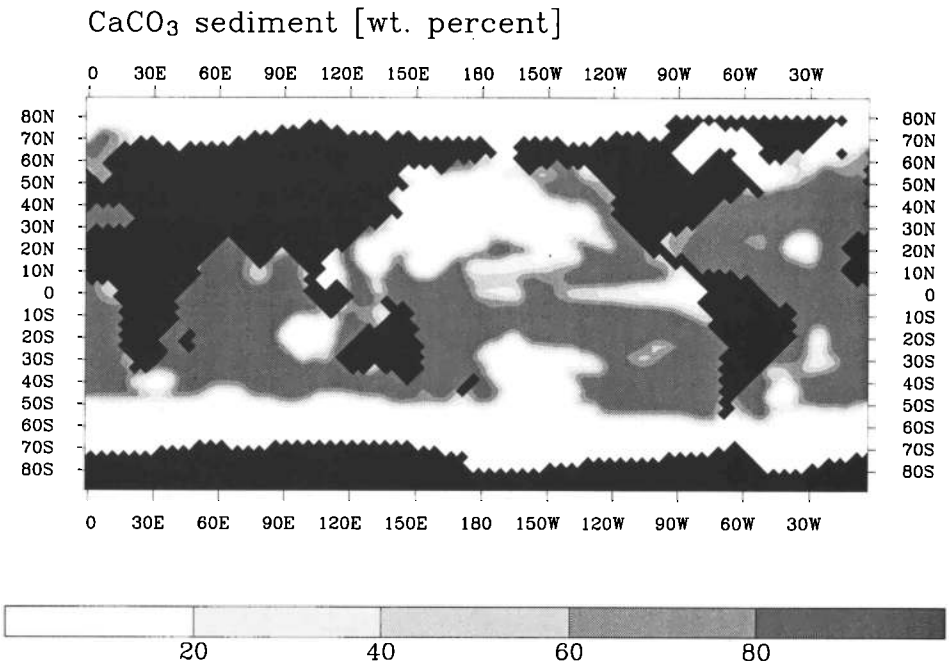

Figure 6. $CaCO_3$ sediment weight percentages as simulated in the control run (average over the entire bioturbated zone).

(a more expensive) trophic model including zooplankton as demonstrated by *Six and Maier-Reimer* [1996]. For the control run the weathering flux of opal into the ocean (as silicic acid) had to be doubled as compared to estimates based on observations [*Tréguer et al.*, 1995] in order to achieve a reasonable standing stock of dissolved $Si(OH)_4$ in the model. This issue can be improved in future studies with the monthly time step model including zooplankton dynamics. The opal belt in the Southern Ocean is reproduced well by the model. This can, however, be due to a possible overestimate of biogenic export production in the model's Antarctic Circumpolar

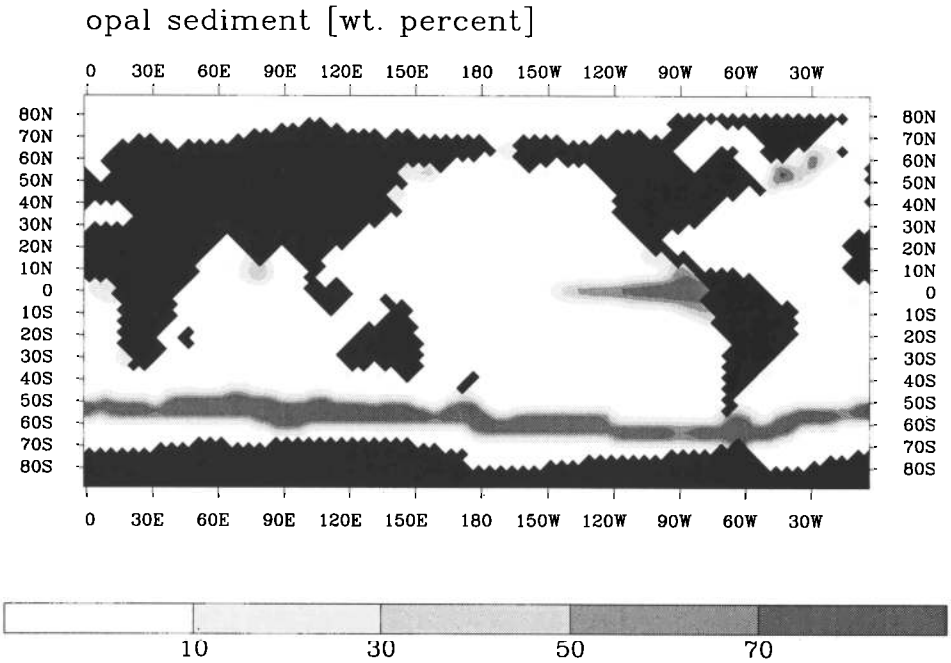

Figure 7. Opal sediment weight percentages as simulated in the control run (average over the entire bioturbated zone).

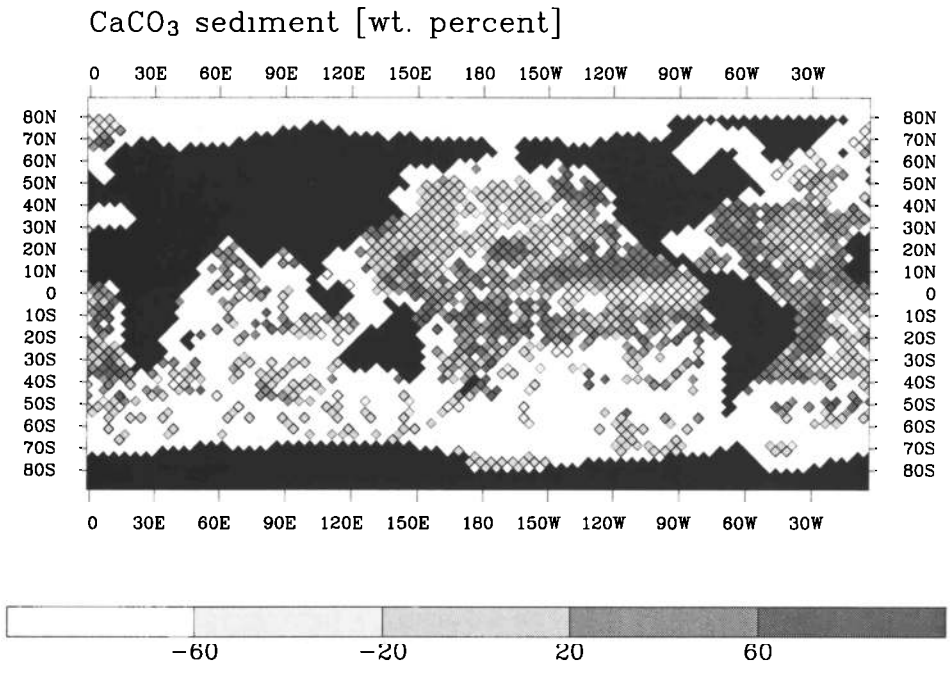

Figure 8. Difference of $CaCO_3$ sediment content model minus observation (in weight percentages). Only the areas marked by squares contain information from observations; at other positions, no observed data are available. (Source of observed data is D. Archer, http://popeye.uchicago.edu/).

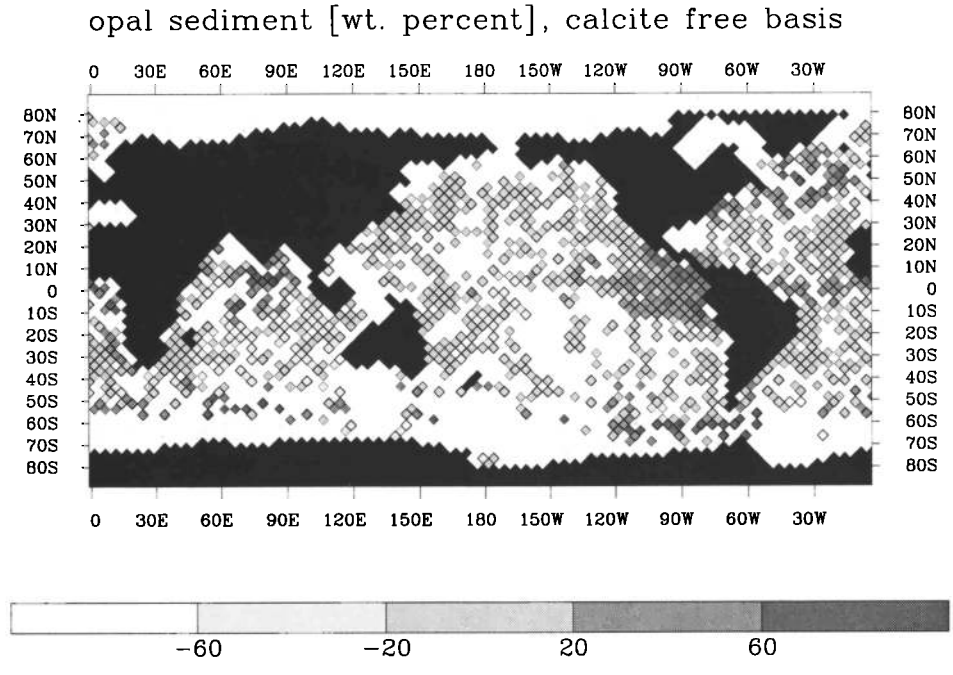

Figure 9. Difference of opal sediment content model minus observation (in weight percentages). Both model and observations were used on a calcite free basis for this comparison. Only the areas marked by squares contain information from observations; at other positions no observed data are available. (Source of observed data is D. Archer, http://popeye.uchicago.edu, based mainly on *Lisitzin* [1971], *Lisitsyn* [1986a, b, c], *Leinen et al.* [1986], and *Lyle et al.* [1988]).

Current (possibly due to a neglect of iron limitation for biological productivity), a region which is not considered as a typical eutrophic region if annually averaged productivity is considered. As mentioned above, the linear dissolution kinetics and the use of a single pore water silicic acid saturation value result in a too strong sensitivity of the opal weight percentage from the local opal rain rate [*Archer et al.*, 1993]. An improved formulation of opal solubility (which is one of the topics within the actual opal research program; see *Raguenau et al.* [1996]) will help to clarify this point. A temperature dependent opal solubility in conjunction with a more differentiating parameterization of opal flux through the water column may improve the actual mechanisms for opal preservation in the model ocean and lead to a diminished opal accumulation in the equatorial Pacific as well as a firm opal preservation in the Southern Ocean, even with a reduced export productivity in this region. The lack of opal sediment in the western North Pacific as seen in observed distibutions [e.g., *Lisitsyn*, 1986a, b, c] is here caused probably by a slight deficiency of the velocity field. In a sensitivity study (see below) it could be demonstrated that by use of an alternative preindustrial velocity field with slightly older North Pacific deep waters, the opal sediment in the western North Pacific is indeed reproduced.

The resulting POC sediment shows significant weight percentages only in selected areas which, in general, coincide with shallow areas and hence significant amounts of organic carbon deposition. This behavior is in rough agreement with observationally based findings [*Jahnke*, 1996]. It must be stated clearly, however, that in nature, organic carbon can be stored within, e.g., cracks of refractory material and then may be unavailable to microbial enzymes. Accumulation of this type of organic carbon is not considered in our model. POC sediment weight percentages thus can be underestimated. The residual of the three biogenic solid sediment compounds is the chemically inert clay sediment which realistically covers the oligotrophic regions, in particular vast areas of the North Pacific (Figure 10). Bulk sedimentation rates (Figure 11) were adjusted by varying the clay flux through the water column to the control run value, so that accumulation rates in oligotrophic regions agree approximately with estimates from observed data (see maps of *Jahnke* [1996]).

The ability of the model to reproduce typical regimes of the oceanic large-scale geochemical status in the water column and sediment is given in plots showing simultaneously the resulting water column profiles for dissolved substances as well as alkalinity, corresponding pore water profiles, solid sediment depth profiles plus $\delta^{13}C$ of sediment $CaCO_3$ and organic carbon (if these substances are available in the respective model sediment) at selected grid points (see location of these points in the map of Figure 12). The North Atlantic "snapshot" (Figure 13) shows that besides $CaCO_3$ and clay, opal is also deposited which, however, gets redissolved within the upper few sediment layers and is not accumulated. The station from the Ross Sea in the Southern Ocean (Figure 14) shows almost complete dominance of opal sediment (except a small weight per-

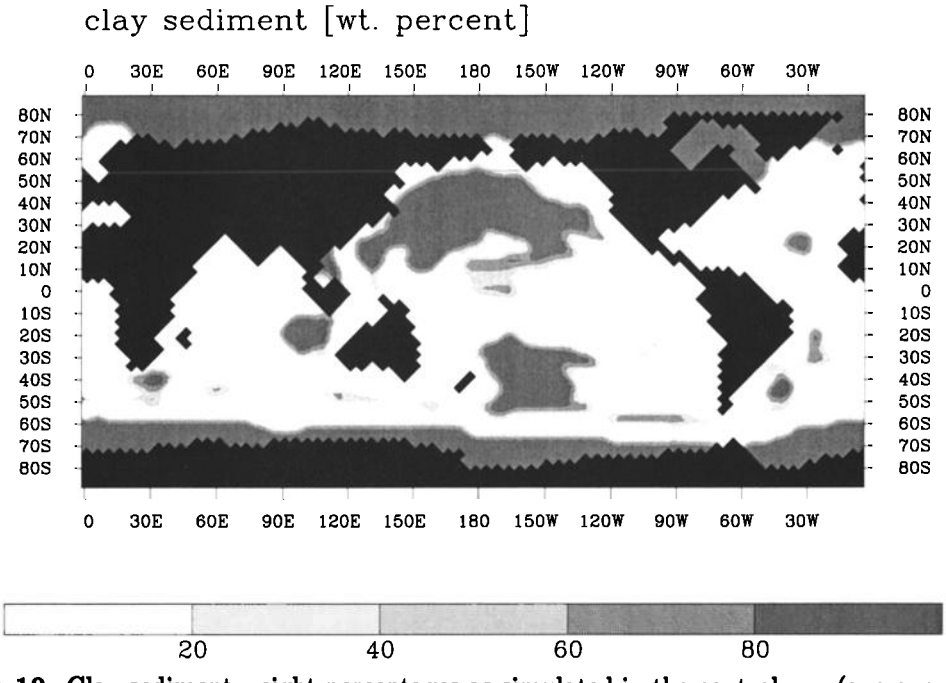

Figure 10. Clay sediment weight percentages as simulated in the control run (average over the entire bioturbated zone).

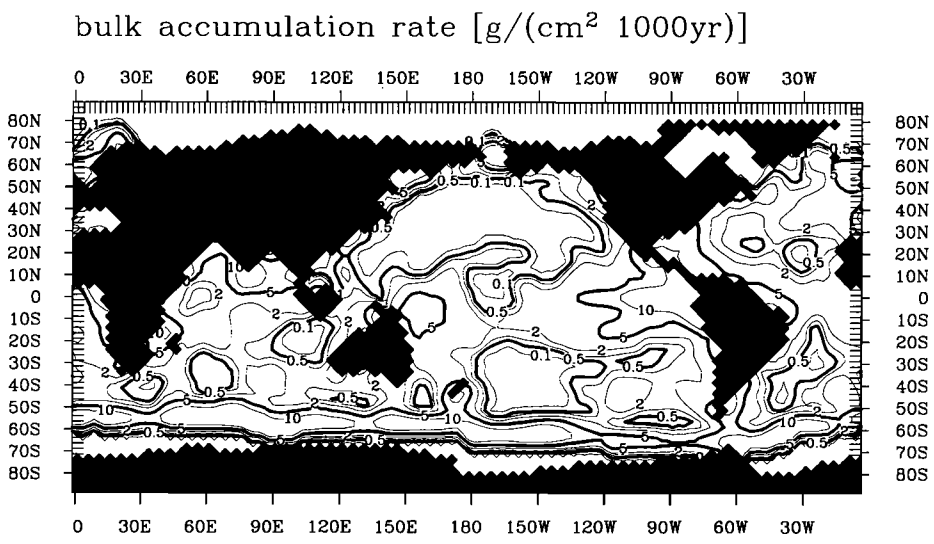

Figure 11. Sediment bulk accumulation rates as simulated in the control experiment (in $g/(cm^2 \times 10^3 years)$).

cent fraction of clay, which is not visible in the plot). The pore water profile for silicic acid shows the typical increase with depth within the sediment and the characteristic asymptotic approach toward the saturation value. A corresponding behavior is also found in observed silicic acid pore water profiles [*Hurd*, 1973; *Vanderborght et al.*, 1977; *Van Bennekom et al.*, 1989; *Archer et al.*, 1993; *Van Bennekom*, 1996]. In the Gulf of Panama, eastern equatorial Pacific, all four sediment components are present. In this nearshore grid point, considerable amounts of organic carbon are deposited and finally accumulated. Oxygen levels within the sediment pore waters decrease to zero within a few centimeters depth in the sediment. Parallel to this, DIC, PO_4^{3-}, and TAlk increase in the sediment pore waters (Figure 15). Comparable oxygen pore water profiles are given by, e.g., *Archer et al.* [1989] as well as *Hales and Emerson* [1996]. Finally, the grid point from the oligotrophic North Pacific provides clear dominance of inert clay material in the solid sediment (Figure 16). Pore water profiles look "boring" owing to only small amounts of reactive biogenic material. A small amount of opal is deposited at this grid point but does not reach the bottom of the bioturbated zone.

4. Sensitivity Experiments

4.1. Change of Clay Flux

The control run result for $CaCO_3$ weight percentage in the bioturbated sediment revealed a tendency toward too high values in the simulation as compared with the measurements (Figures 6 and 8). We examine whether

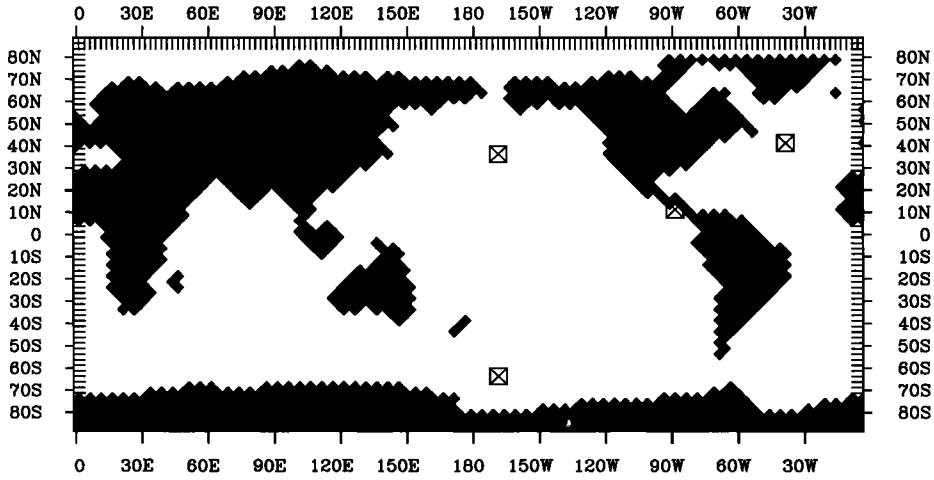

Figure 12. Position of grid points at which local water column and sediment distributions are shown in Figures 13-16.

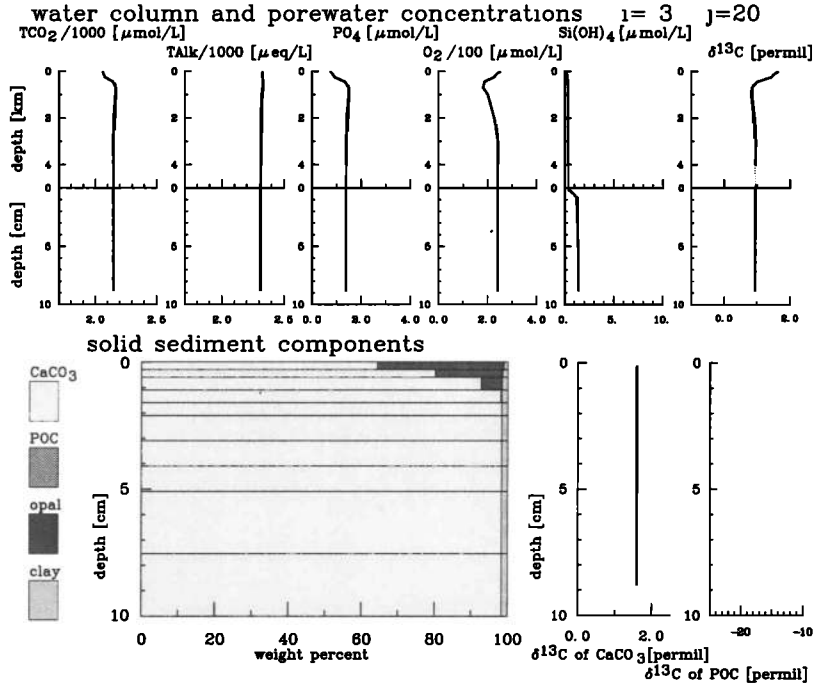

Figure 13. Water column and sediment pore water concentrations as well as solid sediment distribution for a grid point in the North Atlantic (see Figure 12) for the control experiment.

this model deficiency could be remedied by a change in the flux of inert material of terrestrial origin, be it either through input from rivers or through dust input from the atmosphere. Therefore, in a sensitivity experiment, the rain rate for clay material was increased by a factor of 100 as compared to the control run value. From the result for $CaCO_3$ sediment (Figure 17) it can be seen that this "dilution" of the biogenic sediment with

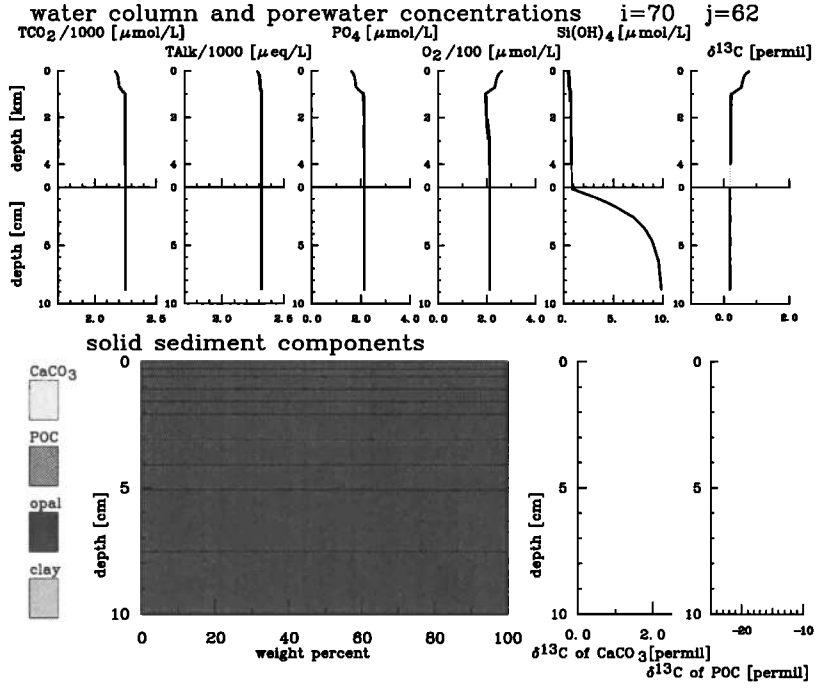

Figure 14. Water column and sediment pore water concentrations as well as solid sediment distribution for a grid point in Antarctic Circumpolar Current (see Figure 12) for the control experiment.

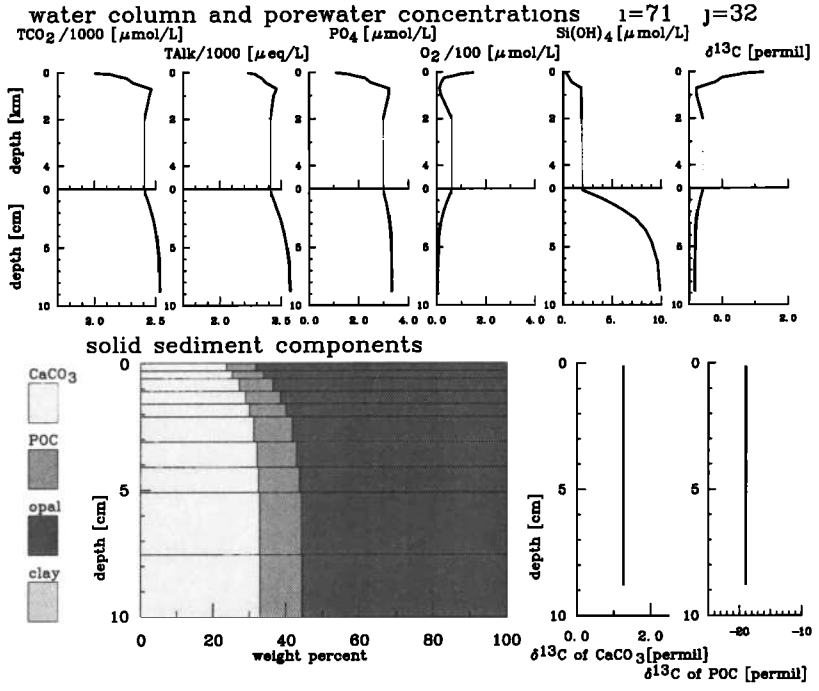

Figure 15. Water column and sediment pore water concentrations as well as solid sediment distribution for a grid point in eastern equatorial Pacific (see Figure 12) for the control experiment.

refractory detritus can be used in "tuning" the overall sediment distribution. The production rates of biogenic particles as well as the atmospheric pCO_2 remain unaffected by this procedure (Table 2). This is important information for future refinements of the model, indicating that an improvement of the particulate flux of terrestrial material can be carried out independently from the subtle biogeochemical balance involving reactive material.

4.2. Change of Bioturbation Rate

The rate of bioturbation, i.e., mixing of solid sediment components through action of infaunal organisms, is discussed as a potentially important factor for control of redissolution of chemically reactive solid sediment compounds [*Schink and Guinasso,* 1977, 1978; *Boudreau,* 1994]. Besides limiting the temporal resolution in sediments due to the stirring action of organisms, their activities may lead, e.g., to enhanced downward mixing of reactive materials into zones of higher pore water saturation and improved preservation. In order to test the influence of a change in the explicit bioturbation of the model on the resulting tracer distributions, this rate was increased by a factor of 10 in one case and decreased by a factor of 10 in the other case. For both cases the model was integrated over 30,000 years, resulting in only negligible changes concerning water column tracer distributions or atmospheric CO_2 concentration (Table 2). Changing the bioturbation has, of course, a significant effect on the relative vertical changes of solid sediment composition within the bioturbated zone as illustrated for the grid point in the Gulf of Panama (Figures 18 and 19; for control run result, see Figure 15). The effect of bioturbation is therefore not important in the model. This finding corroborates the result from *Archer,* [1996] that the required rain ratio of deposited material in order to achieve the observed $CaCO_3$ sediment distribution is insensitive to changes in the bioturbation rate. This insensitive behavior may change if a refined formulation for the kinetics of redissolution and remineralization would be used, and reaction rates would be extremely low. Then material brought down to greater depth within the bioturbated zone could be better preserved. The vertical resolution of several layers of sediment, however, is justified also with the apparent insensitvity to the bioturbation rate because of the differential pore water concentrations and the approach of saturation values in a certain depth within the bioturbated zone. These concentrations determine (besides the rain rate) the rate of redissolution and remineralization of deposited material and therefore, eventually, the accumulation rates.

4.3. Change of POC Flux Profile

In the control run an exponential flux profile was used to redistribute the export production of POC over the water column in order to simulate the vertical particulate flux through the water column. The profile was chosen so that at 770 m depth the POC flux is reduced to $1/e$ [see *Volk and Hoffert,* 1985]:

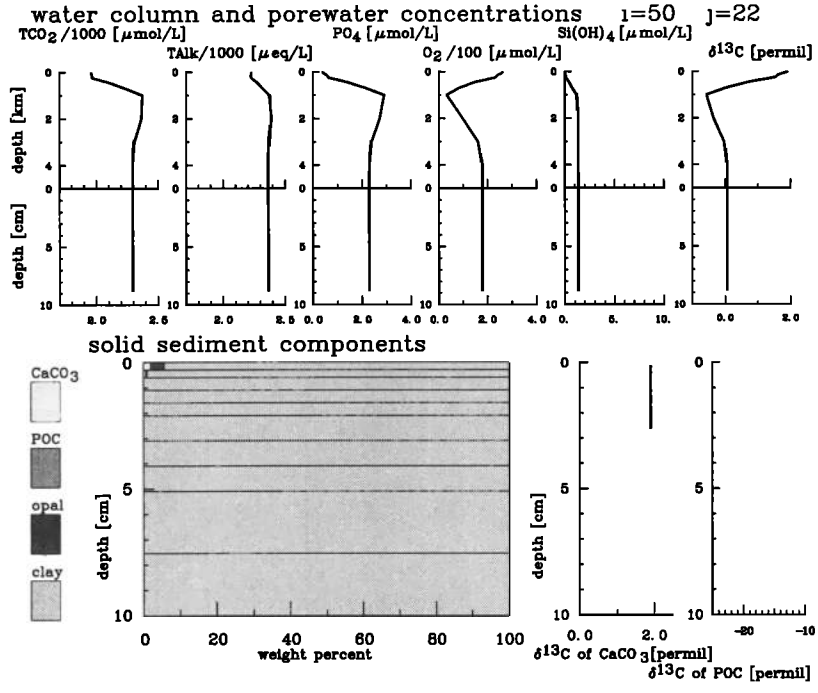

Figure 16. Water column and sediment pore water concentrations as well as solid sediment distribution for a grid point in the oligotrophic North Pacific (see Figure 12) for the control experiment.

$$F(z) = C_{\text{prod}}\, e^{-z/770\text{m}} \qquad (8)$$

where $F(z)$ is the POC flux as a function of depth, C_{prod} is the export production rate of POC, and z is depth in meters.

Alternatively, the POC flux formulation after *Martin et al.* [1987] was tested in a 50,000-year-long integration. This POC flux formula describes the particle flux as a power law, depending on the flux of POC in 100 m water depth (F_{100}):

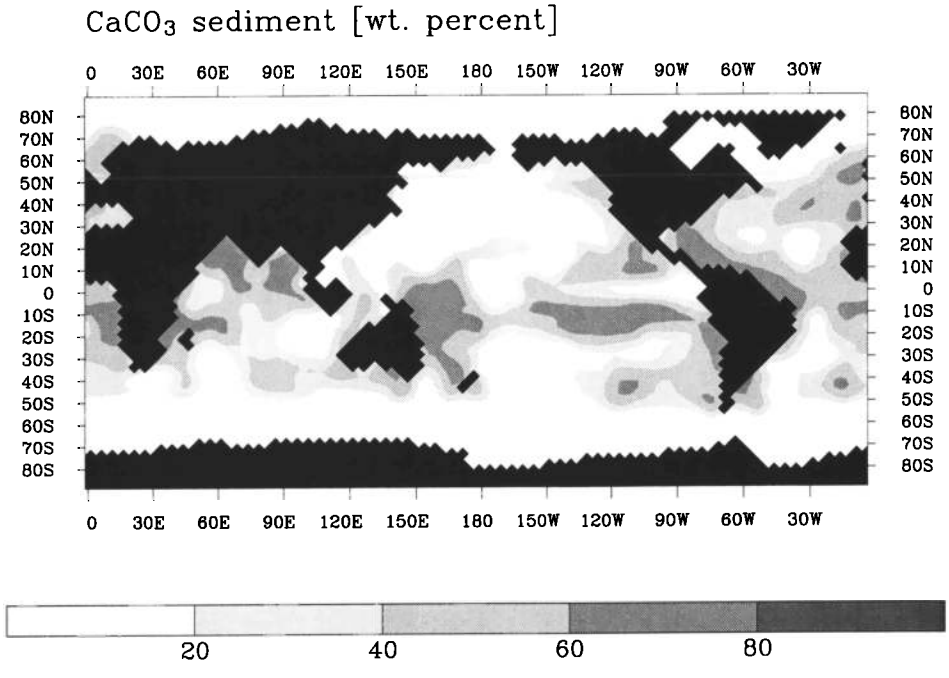

Figure 17. $CaCO_3$ sediment weight percentages averaged over the entire bioturbated zone for the experiment with a 100-fold clay flux as compared to the control run.

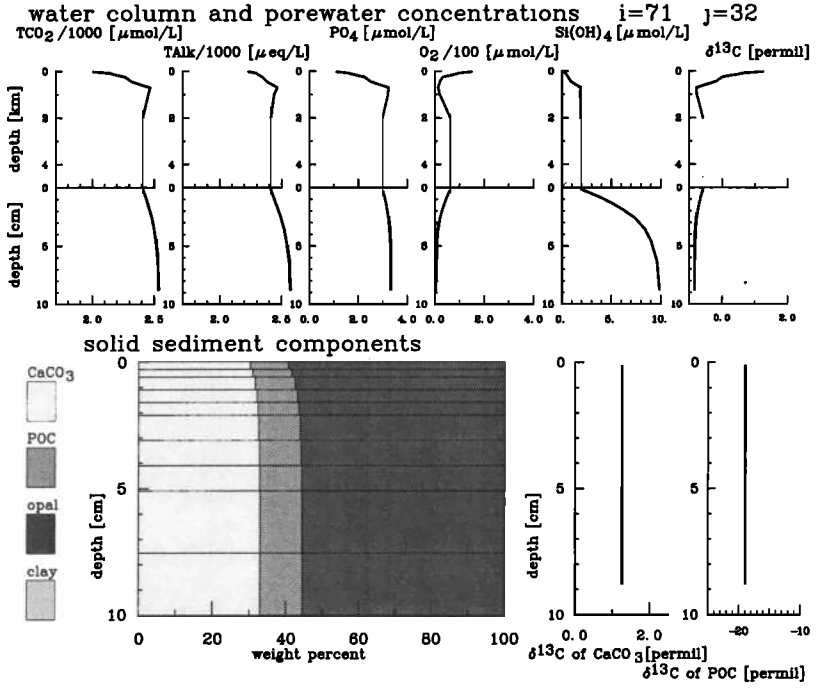

Figure 18. Water column and sediment pore water concentrations as well as solid sediment distribution for a grid point in the eastern equatorial Pacific (see Figure 12) for the experiment with the bioturbation rate decreased to 1/10.

$$F(z) = F_{100}\left(\frac{z}{100}\right)^{-0.858}; \quad z \geq 100\,\mathrm{m} \qquad (9)$$

The differences between both flux parameterizations are illustrated in Figure 20. At first glance these differences appear to be highest in the upper 1 km of the water column. In the deep sea, however, relative deviations of both curves are of about 1 order of magnitude as can be seen by increasing the scale of the x

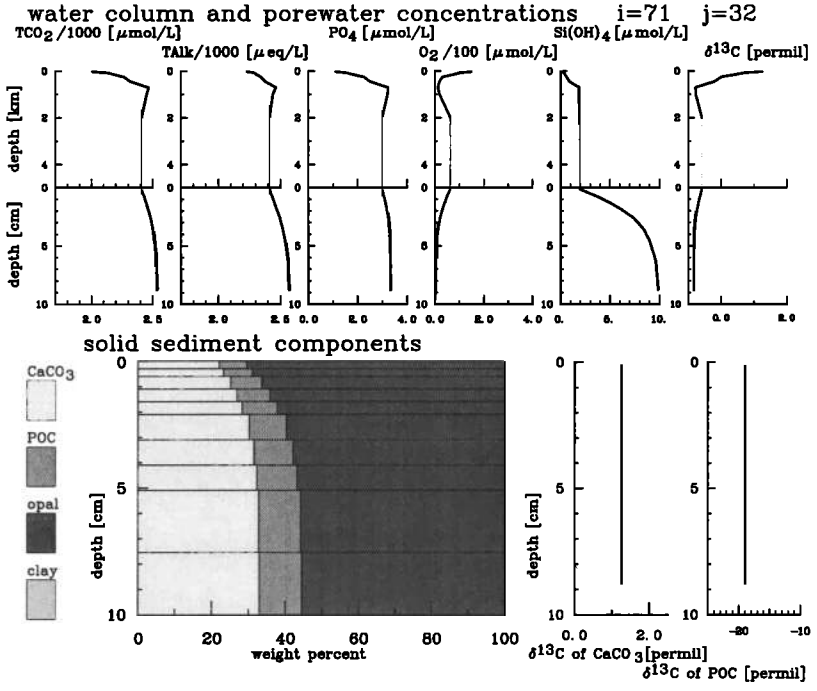

Figure 19. Water column and sediment pore water concentrations as well as solid sediment distribution for a grid point in the eastern equatorial Pacific (see Figure 12) for the experiment with a tenfold increase of bioturbation rate.

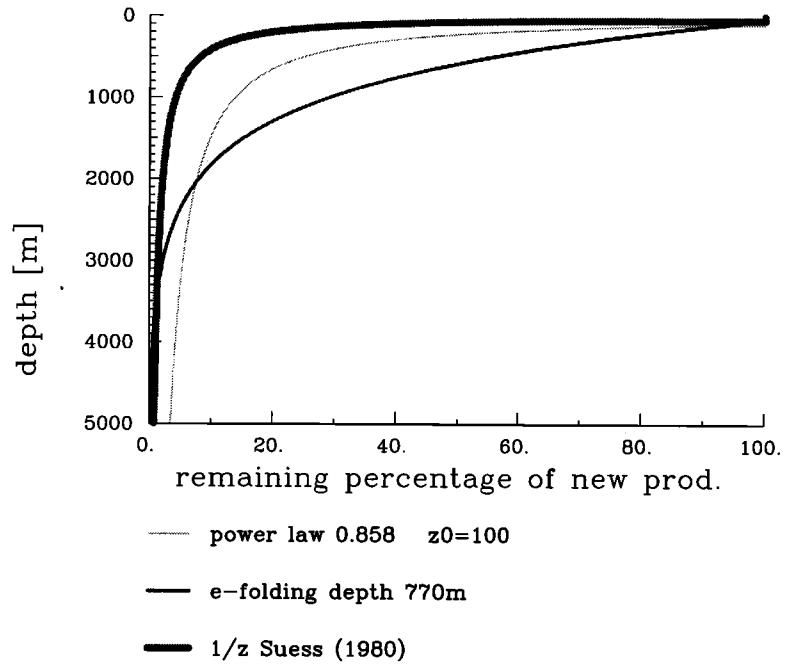

Figure 20. Three different parameterizations for the organic carbon flux through the water column after *Suess* [1980] (thick line), *Volk and Hoffert* [1985] (medium line), and *Martin et al.* [1987] (thin line), given as percentage of export production versus depth.

axis in the diagram (Figure 21). In quasi-equilibrium, use of the *Martin et al.* [1987] formulation here leads to slight changes in the production rates of POC and consequently also in $CaCO_3$ as well as a small increase in atmospheric pCO_2 (Table 2). In view of these numbers the flux curve would be perfectly acceptable. As may be expected from Figure 21, the deposition of POC to the top sediment layer increased strongly, leading to an unrealistically high amount of organic carbon in the sediment of the equatorial Pacific Ocean. For the con-

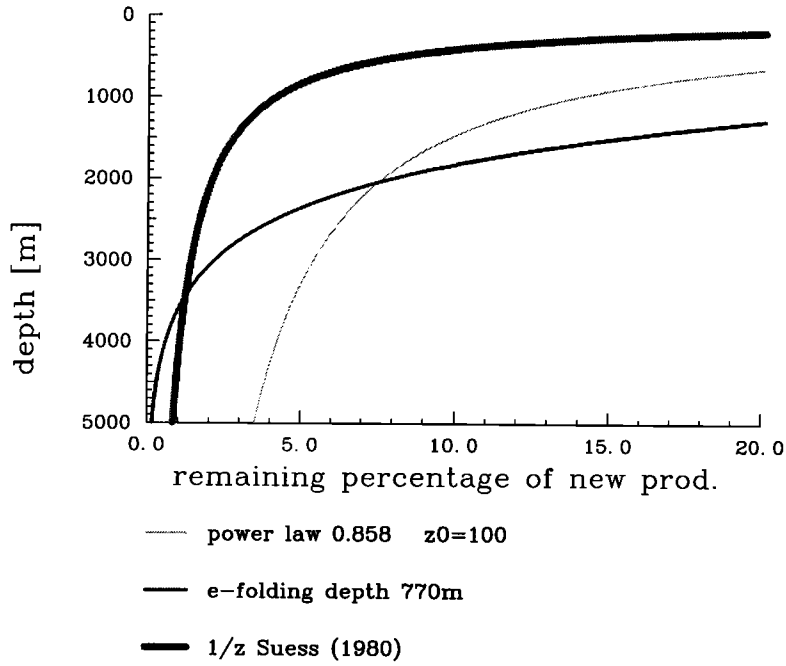

Figure 21. Same as Figure 20, but with stretched x axis in order to resolve better the deep-sea distribution.

trol run configuration the POC flux parameterization turned out to be incompatible with the other parameterizations of processes.

In a further sensitivity experiment the POC flux formula according to *Suess* [1980] was used:

$$F(z) = \frac{C_{\text{prod}}}{0.0238\, z + 0.212}; \quad z \geq 50\,\text{m} \quad (10)$$

Compared with the other POC flux parameterizations, this function predicts a shallower recycling of POC (Figures 20 and 21). This flux formulation here leads to unstable conditions for the resulting atmospheric pCO_2. The integration was stopped after a few thousand years of integration and an atmospheric CO_2 value approaching 1000 ppm. This behavior is due to a decoupling of the POC and $CaCO_3$ as well as opal fluxes. The shallower recycling of POC leads to an increase in POC new production. The opal production cannot increase in parallel because the opal flux parameterization was not changed. The enhanced POC production, rather, is parallel with an increase in $CaCO_3$ production, leading to a reduction of surface ocean alkalinity, which increases the atmospheric CO_2 partial pressure (Table 2). For biogenic particulate matter the globally averaged rain ratio of $C(CaCO_3)$:C(POC) increases from 0.2 for the control run to 0.33 for the run with the *Suess* [1980] POC flux formulation. The corresponding rain ratio of Si(opal):C(POC) decreased from 0.02 to 0.01 (Table 2).

Further studies have to be carried out in order to clarify whether an alternative POC flux formulation can be used if other model parameters and process representations are also adjusted and modified. At this point it appears premature to reject one or the other parameterization solely on the basis of the model results.

4.4. Change of Rain Ratio

In order to test the sensitivity of the model results with respect to the rain ratio formulation (equation (5)), the threshold value S_{opal} for the start of $CaCO_3$ production was decreased by 10%. This leads to a further reduction of silicic acid in surface waters until $CaCO_3$ production starts. The overall effect is a moderate atmospheric CO_2 reduction of 22 ppm due to the resulting shift of the average $C(CaCO_3)$:C(POC) rain ratio from 0.2 to 0.17 in conjunction with a respective sea surface alkalinity increase compared with the control run (Table 2). As the model reacts sensitively to small changes of the rain ratio, the governing natural processes need to be identified more thoroughly from observations.

4.5. Change of Opal Solubility: ($Si(OH)_4$ Pore Water Saturation Value)

The influence of a change in the $Si(OH)_4$ saturation value with respect to opal, i.e., the solubility of opal within the sediment pore waters, was investigated in two model runs where this saturation value was halved to 500 μmol/L (50% solubility decrease) and doubled to 2000 μmol/L (twofold solubility increase) as compared with the control run. While the POC export production values remain unaffected by this, strong changes in $CaCO_3$ production, opal production, and atmospheric pCO_2 result. Responsible for the pCO_2 change is primarily, again, an inferred rain ratio shift with high calcite production plus high pCO_2 and low opal production on one side and low calcite production plus low pCO_2 and high opal production on the other side (Table 2). Through enhanced redissolution of opal from the sediment, in the model, the atmospheric pCO_2 can be strongly changed through the alteration of the water column concentrations of $Si(OH)_4$, DIC, and TAlk paralleling changes in the biogenic particle composition. In fact, the deep-sea silicic acid concentration in the model is primarily determined by the redissolution strength of opal from the sediment (Figure 22). The opal solubility therefore could be used to improve the too low water column deep sea $Si(OH)_4$ concentrations in the control run. The DIC and TAlk changes that are associated with the change in opal solubility (Figure 22) and the implied pCO_2 change underline the necessity for an improved understanding of Si cycling in view of geochemically induced natural climate variability.

4.6. Change of Velocity Field

Running the sediment model with different velocity fields is important for two reasons: (1) as a model test, in order to see whether distributions of tracers remain reasonable, and (2) for paleoceanographic applications, in order to use the composition of solid sediment material for validations of reconstructions of past oceans. An example of such applications is already available for model velocity fields from the Hamburg LSG-OGCM [*Mikolajewicz et al.*, 1993] with different tectonic boundary conditions, i.e., an open Panama isthmus (as one feature of the Miocene ocean) and a case with open Panama isthmus plus, in addition, a closed Drake Passage, which may represent some similarity with the early Oligocene ocean. Corresponding carbon cycle plus sediment model runs, relative to a control run using the preindustrial standard velocity field of *Maier-Reimer et al.* [1993] are given by *Heinze and Crowley* [1997]. This second control (C2) run gives an ideal opportunity to test the validity of the sediment model for a slightly different preindustrial velocity field as used for the standard run C1 in this paper (see Table 2). Besides this second preindustrial velocity field, we present model results for a first attempt to realistically reconstruct the oceanic circulation at the last glacial maximum as presented by *Winguth et al.* [1996]. This glacial velocity field is directly comparable with the control run C1 used basically in this manuscript.

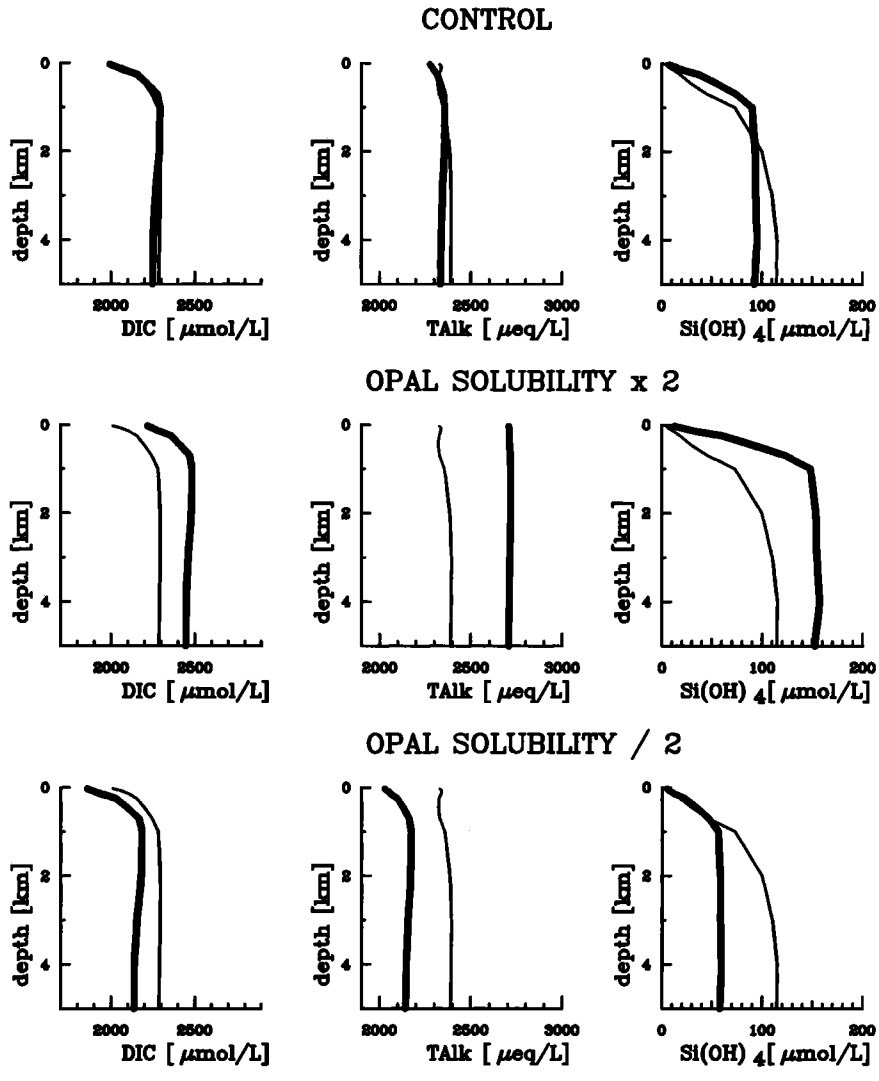

Figure 22. Comparison of the modeled (thick lines) and observed (thin lines, GEOSECS data) mean water mass property depth profiles for the control run and the sensitivity experiments with changes in the $Si(OH)_4$ saturation value for opal in sediment pore waters.

4.6.1. Second run for the preindustrial ocean. In order to provide a basis for comparison of already existing carbon cycle model runs with the annually averaged model [*Heinze et al.*, 1991; *Heinze and Crowley*, 1997], a second preindustrial control run (C2) was carried out by use of the same velocity field on which those studies have been based. In order to achieve an atmospheric CO_2 concentration close to the preindustrial level of 280 ppm, only one model parameter was changed for run C2 as compared with C1, namely, the threshold ratio of Si(opal):C(POC) for gradual start of $CaCO_3$ production (S_{opal} in (5) was modified from 0.35506 to 0.43005), resulting in a quasi-equilibrium value for atmospheric pCO_2 of 283 ppm for experiment C2.

Resulting distributions for $CaCO_3$ and opal sediment are given in Figures 23 and 24. As already shown by *Heinze and Crowley* [1997], the opal sediment distribution (here additionally reproduced in black and white and the same shading as used for experiment C1) with the use of a velocity field after *Maier-Reimer et al.* [1993] provides a significant buildup of biogenic opal sediment in the western North Pacific (compare Figures 24 and 7) plus a westward extension of the equatorial Pacific opal belt. Also, the $CaCO_3$ sediment distribution differs between runs C1 and C2 (Figures 23 and 6), where the velocity field used in experiment C2 reveals a tendency toward stronger corrosion, especially visible in the Indian Ocean. The major sediment distribution features are robust for run C1 and C2, such as the dominance of $CaCO_3$ in the Atlantic Ocean as well as the high opal amounts in the Southern Ocean and the equatorial Pacific regime. The western North Pacific opal sediment is reproduced only in C2 and not

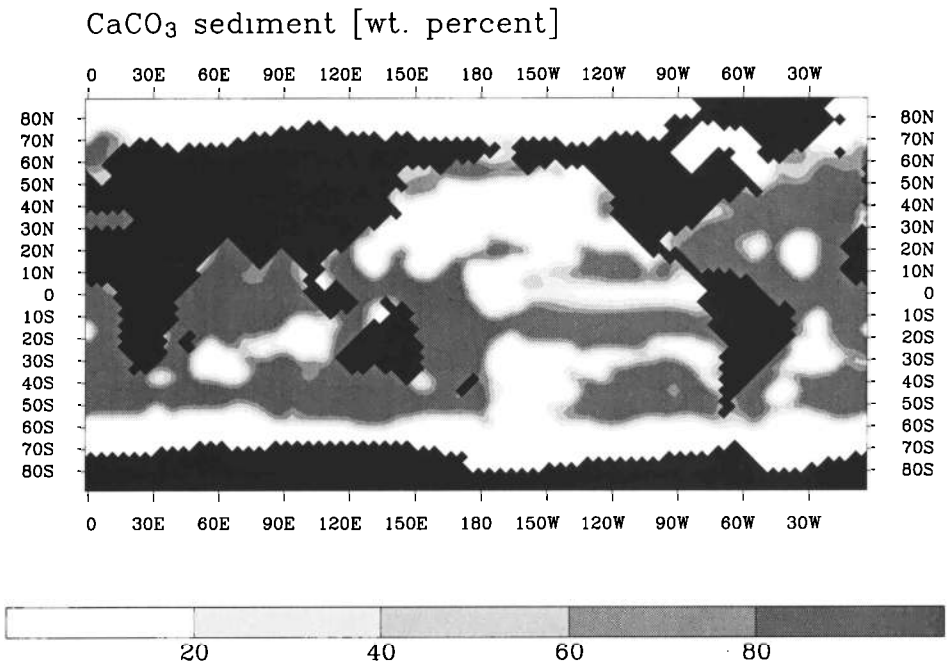

Figure 23. $CaCO_3$ sediment weight percentages as simulated by use of the preindustrial velocity field of *Maier-Reimer et al.* [1993] (average over the entire bioturbated zone).

in C1, indicating that this region may be very sensitive for slight changes in ocean circulation, which may have important implications for paleoceanographic studies in this area.

4.6.2. Glacial ocean. The glacial velocity field of *Winguth et al.* [1996] already shows remarkable agreement between simulated and observation based glacial $\delta^{13}C$ patterns in the water column, in particular, a weakening of North Atlantic Deep Water (NADW) production and farther northward intrusion of Antarctic Bottom Water in the Atlantic [see also *Winguth,* 1997]. It is also intriguing to use this velocity field in the full

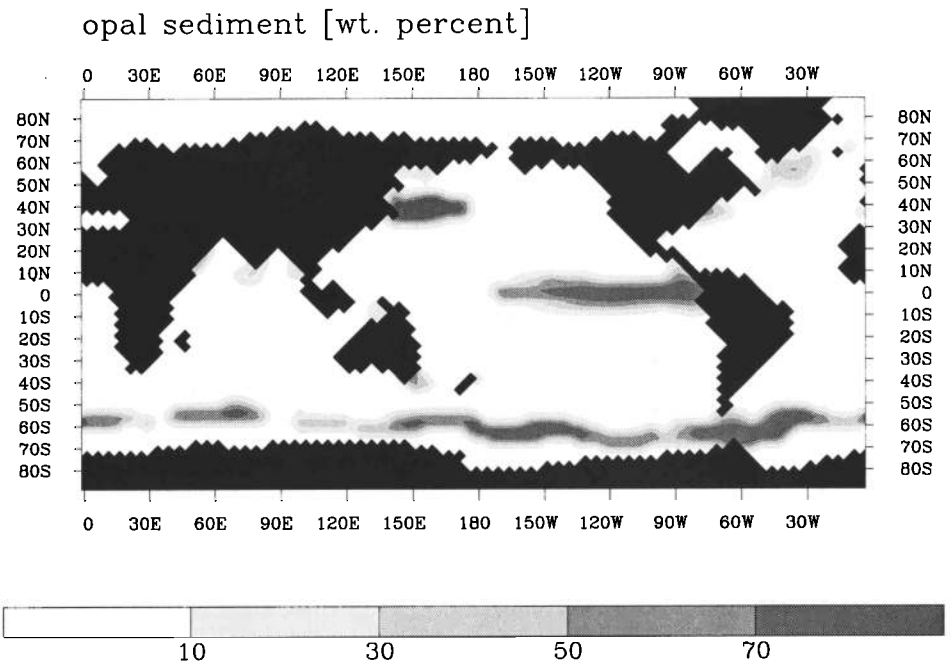

Figure 24. Opal sediment weight percentages as simulated by use of the preindustrial velocity field of *Maier-Reimer et al.* [1993] (average over the entire bioturbated zone).

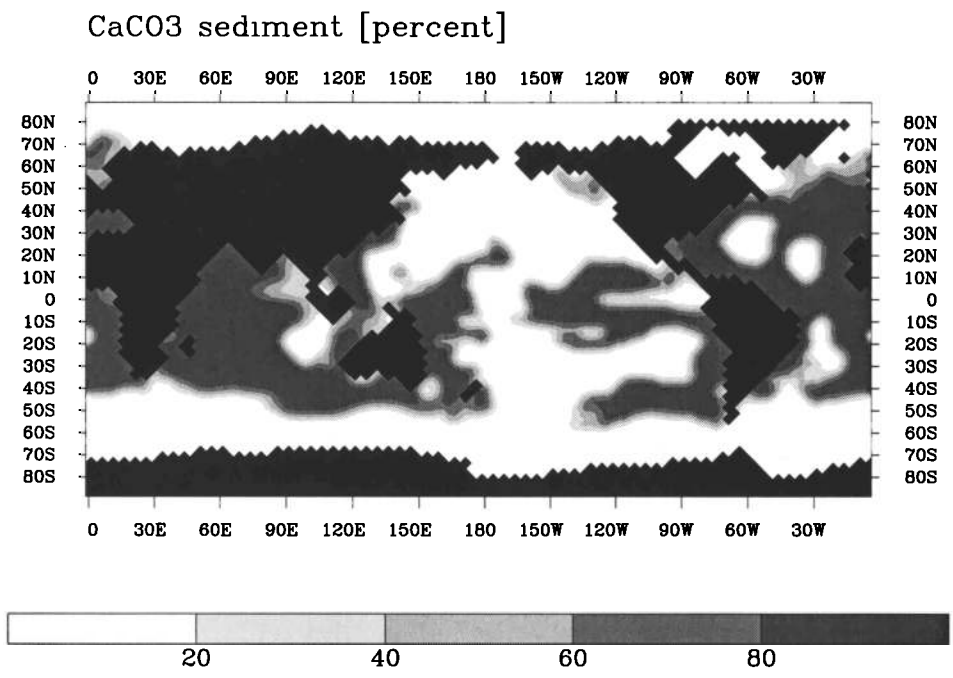

Figure 25. $CaCO_3$ sediment weight percentages as simulated by use of the glacial velocity field of *Winguth et al.* [1996] (average over the entire bioturbated zone).

geochemical model in order to check the ability of the sediment model to reproduce different "sediment climate" states.

Restarting from the control distributions of C1, the geochemical model was integrated over a period of 100,000 years after switching instantaneously from preindustrial ("interglacial") to glacial velocity and thermohaline fields. All model parameters were kept at identical values to the control run (see Table 1). Resulting sediment distributions for $CaCO_3$ and opal weight percentages plus corresponding glacial–preindustrial differences are given in Figures 25 – 28.

Some characteristic changes for the glacial sediment distribution compared with the preindsutrial situation have been inferred from sediment core analysis. $CaCO_3$ corrosivity in the North Atlantic was higher, especially in the deep western boundary current regime off the east coast of North America [*Balsam,* 1983; *Crowley,* 1983, 1985], in contrast to a tendency toward better $CaCO_3$ preservation in the Indian and Pacific Oceans [*Peterson*

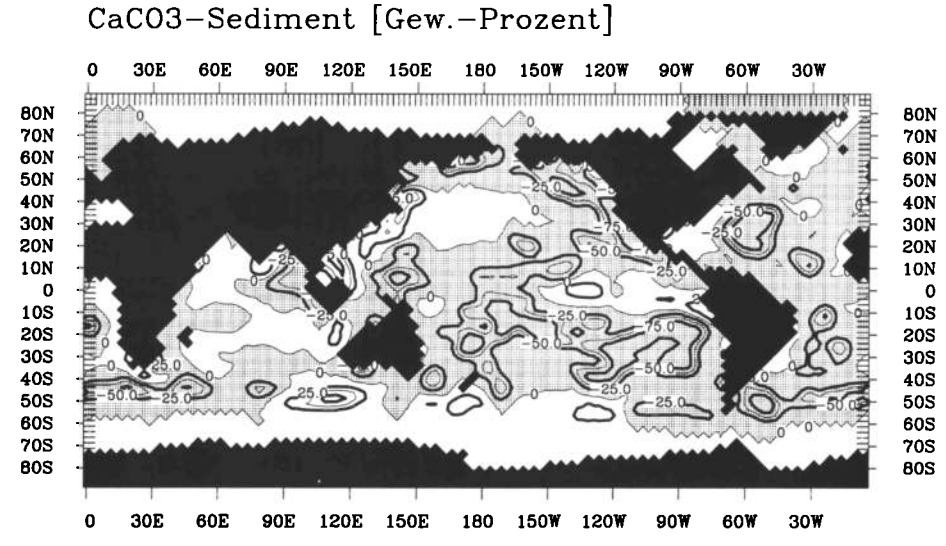

Figure 26. Difference of $CaCO_3$ sediment (in weight percentages) glacial minus preindustrial values. (Negative values are shaded.)

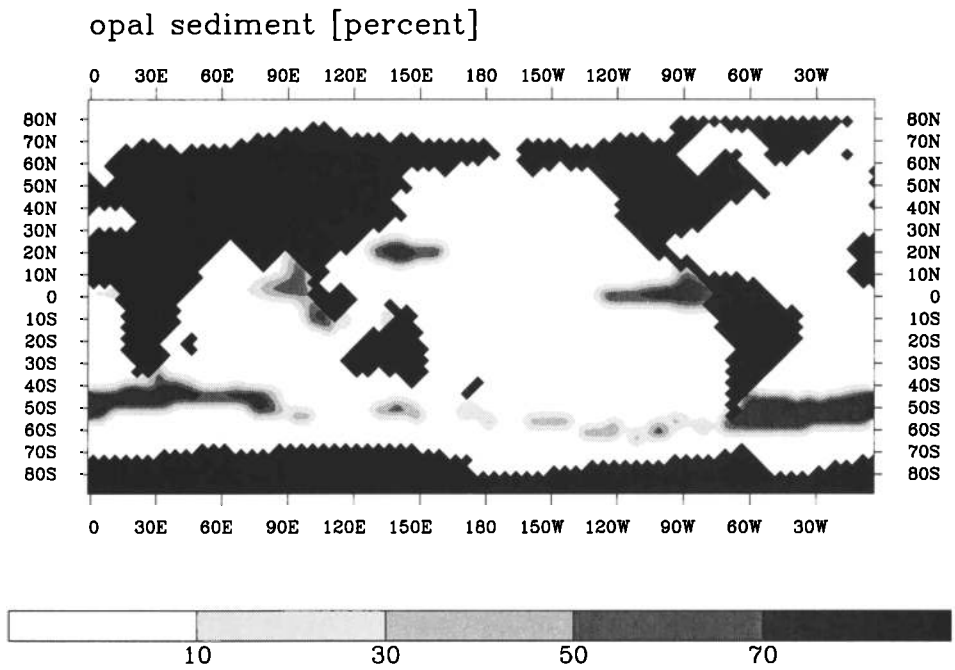

Figure 27. Opal sediment weight percentages as simulated by use of the glacial velocity field of *Winguth et al.* [1996] (average over the entire bioturbated zone).

and Prell, 1985; *Farrell and Prell,* 1989, 1991]. A shift of the opal accumulation belt in the Atlantic sector of the Antarctic Circumpolar Current with stronger accumulation north of the position of today's polar front zone (at 50°S) and reduced accumulation south of this line is described by *Charles et al.* [1991], *Mortlock et al.* [1991], and *Kumar et al.* [1995]. A similar shift was also observed for the Indian Ocean part of the Southern Ocean [*Charles et al.,* 1991].

Glacial model results for the Atlantic show good agreement with observed trends, with a clear $CaCO_3$ sediment reduction in the North Atlantic with realistic emphasis on the west side of the basin (Figure 26). Also, the north-south opal fractionation in the Atlantic sector of the Southern Ocean is reproduced by the model, as a consequence of glacial equatorward shift of sea ice cover (Figure 28). The model fails, however, to reproduce the same north-south fractionation of opal sediment in the

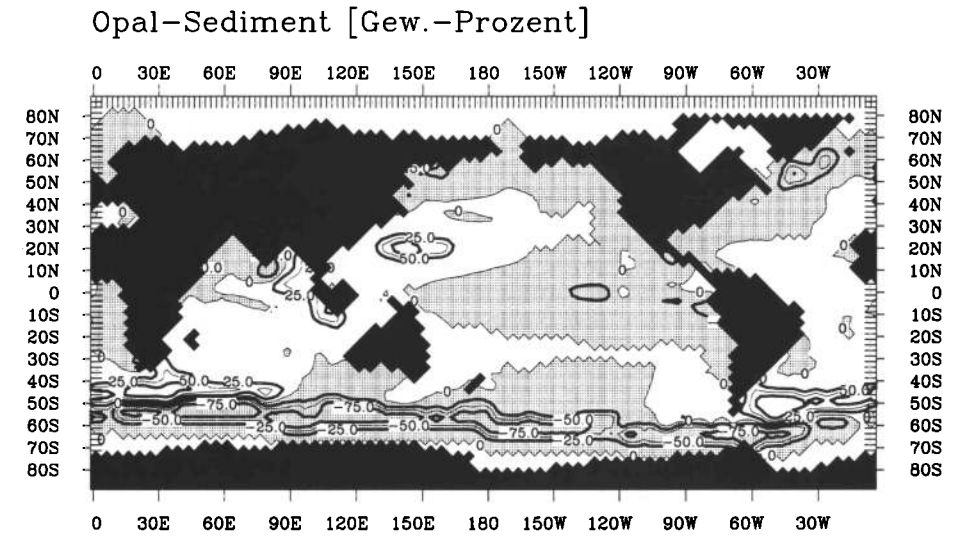

Figure 28. Difference of opal sediment (in weight percentages) glacial minus preindustrial values. (Negative values are shaded.)

Indian Ocean part of the Antarctic Circumpolar Current area. There, the model, in contrast to observations, yields a $CaCO_3$ maximum south of Australia. This discrepancy is probably the result of large uncertainties in the surface boundary conditions for the last glacial maximum. In the Pacific the model does not show the large-scale trend toward an improved $CaCO_3$ preservation. An exception is the central and eastern equatorial Pacific, where the model also indeed shows a relative increase of $CaCO_3$ sediment.

Overall, from the sediment model approach, the glacial model ocean circulation for the Atlantic Ocean shows good agreement with evidence from the geological record, while for the Indian and Pacific Oceans, discrepancies remain. The partly unrealistic sediment distribution in the Indo-Pacific sector of the Antarctic Circumpolar Current indicates that the model deficiencies may be linked to the bottom water formation mechanism in this region. Unfortunately, even for today's ocean, forcing fields for the south polar area are not well established compared with areas with much higher spatial and temporal meteorological data coverage. At least the coincidence of an acceptable $\delta^{13}C$ and sediment cover simulation for the glacial Atlantic is encouraging and a partial validation for the sediment model. The resulting pCO_2 for the glacial ocean increases unrealistically to 312 ppm in contrast to ice core measurements [*Barnola et al.*, 1987; *Staffelbach et al.*, 1991]. Also, in other OGCM studies, the pCO_2 shift due to changes in the oceanic velocity field was too small in order to explain the observed change [*Heinze*, 1990; *Heinze et al.*, 1991; *Winguth*, 1997]. The second stable mode circulation, which was used by *Heinze et al.* [1991], also showed zero-order agreement with reconstructed $\delta^{13}C$ water column values for the last glacial maximum. With the former carbon cycle model version as used by *Heinze et al.* [1991], i.e., without chemically active multilayer sediment, a slight reduction of atmospheric pCO_2 by 9 ppm could be achieved [see *Heinze et al.*, 1991]. In our experiment, with a comparable glacial $\delta^{13}C$ distribution, in constrast to the former study, a significant increase in atmospheric pCO_2 results. This different behavior can be explained by the fact that owing to the chemically active sediment model, the total chemical inventories can vary though input and output of matter are balanced. In this sense the present model is more sensitive than the previous one that was applied by *Heinze et al.* (1991).

Assuming that the sediment model is, to first order, reproducing processes correctly, the result for the glacial pCO_2 may indicate that the Pacific part of the glacial ocean velocity fields needs more refinement. Furthermore, the too strong $CaCO_3$ corrosion in the modeled Indo-Pacific regime shows that the alkalinity in this area is too low in the simulation. One option to improve the situation here would be to change the input of weathering fluxes toward an incrase of alkalinity input as suggested by *Archer and Maier-Reimer* [1994] and *Munhoven and François* [1996]. As a final experiment therefore the weathering input of opal and alkalinity (CO_3^{2-}) was increased by a factor of 1.5, corresponding in an absolute sense approximately to the doubling of riverine Si fluxes during the glacial as suggested by *Froelich et al.* [1992], in view of the two high opal input rates through weathering as chosen for the control run. This procedure lowers the pCO_2 for the glacial velocity field from 312 to 218 ppm primarily due to an alkalinity increase. This rise of TAlk, however, has the effect of making the Atlantic Ocean too preserving with respective to $CaCO_3$ rendering an unrealistically pronounced glacial $CaCO_3$ sediment (Figure 29).

5. Summary

A 10-layer sediment module was coupled to an existing geochemical OGCM, which is able to reproduce large-scale fluxes of carbon and silicon in the world ocean. Si and C cycles are coupled in the model through a formulation for the "rain ratio" Si:C(POC):C($CaCO_3$). The model is fast enough to be integrated over several ten thousands of years. Water column tracer distributions, pore water concentrations, and weight percentages of four solid sediment components can be simulated qualitatively by use of velocity fields for the preindustrial ocean.

Parameter sensitivity studies confirm that the input of nonreactive terrestrial particulate matter is not important for the distributions of geochemical tracers in the water column or even the atmospheric CO_2 partial pressure and can be used for appropriate tuning of the simulated distributions of biogenic matter in the sediment. A better knowledge of this flux, however, is necessary in order to model correctly concentrations of reactive sediment components. The deposition rate of POC to the seafloor is of vital importance for the simulation of organic carbon sediment. The model reacts very sensitively to changes of the parameterizations of the POC flux through the water column, giving better results for an exponential flux profile than for a power law formulation. This does not necessarily mean that one parameterization is better than the other in an absolute sense. It, rather, points out the difficulties in getting the correct particulate fluxes and sediment distributions simultaneously. The Joint Global Ocean Flux Study (JGOFS) database will be one of the basic tools for improving this part of the model. Necessary improvements of the model especially concern the mechanisms of opal preservation and dissolution. A further analysis also has to be carried out for the "rain ratio" Si:C(POC):C($CaCO_3$) on the basis of available and fu-

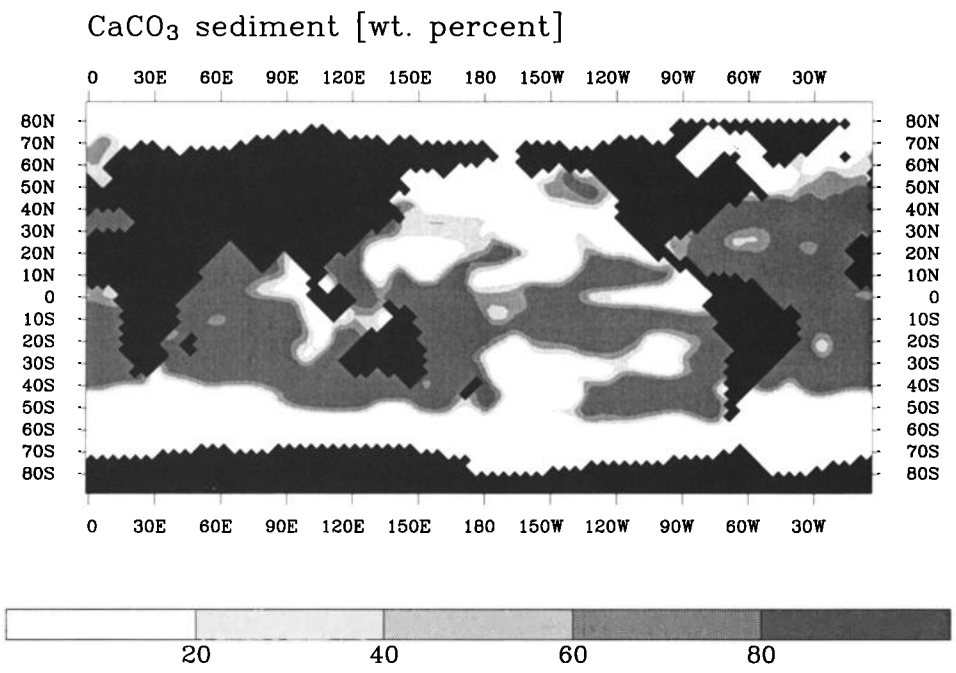

Figure 29. $CaCO_3$ sediment weight percentages as simulated by use of the glacial velocity field of *Winguth et al.* [1996] using a 50% increase of opal and CO_3^{2-} input to the ocean through weathering (average over the entire bioturbated zone).

ture data, because this is the interface which effectively couples the Si and C cycling in the marine environment. The solubility of opal turned out to be one of the most important factors in governing the oceanic silicic acid inventory. Through the coupling of the Si and C cycles via the biogenic particle production, the redissolution rate of opal from the sediment also has potentially a considerable impact on the atmospheric CO_2 concentration.

For a glacial ocean velocity field, results from $\delta^{13}C$ can be substantiated by the resulting sediment patterns. The glacial Atlantic can be reproduced fairly well, while for the Indian and Pacific Oceans, considerable discrepancies remain, in particular, a shift toward stronger $CaCO_3$ dissolution. This disagreement and the simulated unrealistic increase of atmospheric CO_2 partial pressure could be reduced by a change of the alkalinity inventory, e.g. through a change of material input from continental weathering. In a study on changes in tectonic boundary conditions [*Heinze and Crowley*, 1997], the model configuration presented here has already proven to be helpful in interpreting and evaluating results of a physical OGCM. Also, for the interglacial-glacial shift, the sediment model turns out to be a useful tool for verifying paleoclimate modeling efforts. Important in the present model configuration is, that linkages between sediment diagenesis, water column properties, and atmospheric CO_2 can be investigated that cannot be derived from isolated sediment modeling studies. One example for such studies is the linkage between opal solubility and atmospheric CO_2. Results from studies that concentrate only on one compartment of the geochemical cycling could not be easily extrapolated to the real system. Tuning of the complex model configuration is a comprehensive and time-consuming task. In view of the difficulties in reconciling prognostically the sediment data, water column tracers, and the atmospheric CO_2 concentration, the model with its basic parameterizations is encouraging. The available model configuration will also help in the use of the wealth of geological data for physical paleoceanographers.

Acknowledgments. We are grateful to the staff of the Deutsches Klimarechenzentrum GmbH (German Climate Computing Center) for invaluable assistance in using the computing facilities. This work was supported by grants Ma1070/2-1 from the Deutsche Forschungsgemeinschaft and MAS3-CT97-0141 (MAST III program) from the European Communities.

References

Archer, D., Modeling the calcite lysocline, *J. Geophys. Res.*, 96(C9), 17,037-17,050, 1991.

Archer, D., A data-driven model of the global calcite lysocline, *Global Biogeochem. Cycles*, 10, 511-526, 1996.

Archer, D., and E. Maier-Reimer, Effect of deep-sea sedimentary calcite preservation on atmospheric CO_2 concentration, *Nature*, 367, 260-263, 1994.

Archer, D., S. Emerson, and C. R. Smith, Direct measurement of the diffusive sublayer at the deep sea floor using oxygen microelectrodes, *Nature*, 340, 623-626, 1989.

Archer, D., H. Kheshgi, and E. Maier-Reimer, Multiple timescales for the neutralization of fossil fuel CO_2, *Geophys. Res. Lett.*, 24, 405-408, 1997.

Archer, D., M. Lyle, K. Rodgers, and P. Froelich, What controls opal preservation in tropical deep-sea sediments?, *Paleoceanography*, 8, 7-21, 1993.

Bacastow, R. B., and E. Maier-Reimer, Circulation model of the oceanic carbon cycle, *Clim. Dyn.*, 4, 95-125, 1990.

Balsam, W. L., Carbonate dissolution on the Muir Seamount (Western North Atlantic): Interglacial/glacial changes, *J. Sediment. Petrol.*, 53, 719-731, 1983.

Barnola, J. M., D. Raynaud, Y. S. Korotkevich, and C. Lorius, Vostok ice core provides 160,000-year record of atmospheric CO_2, *Nature*, 329, 408-414, 1987.

Berner, R. A., A. C. Lasaga, and R. M. Garrels, The carbonate-silicate geochemical cycle and its effect on atmospheric carbon dioxide over the past 100 million years, *Am. J. Sci.*, 283, 641-683, 1983.

Boudreau, B. P., Is burial velocity a master parameter for bioturbation? *Geochim. Cosmochim. Acta*, 58, 1243-1249, 1994.

Boudreau, B. P., Diagenetic Models and Their Implementation, 414 pp., Springer-Verlag, New York, 1997.

Boyle, E. A., The role of vertical chemical fractionation in controlling late Quaternary atmospheric carbon dioxide, *J. Geophys. Res.*, 93, 15,701-15,717, 1988.

Broecker, W. S., and T.-H. Peng, Tracers in the Sea, 690 pp., Lamont-Doherty Earth Observatory, Palisades, N.Y., 1982.

Broecker, W. S., and T. Takahashi, Neutralization of fossil fuel CO_2 by marine calcium carbonate, in The Fate of Fossil Fuel CO_2 in the Oceans, edited by N. R. Anderson and A. Malahoff, pp. 213-241, Plenum, New York, 1977.

Broecker, W. S., S. Sutherland, W. Smethie, T.-H. Peng, and G. Östlund, Oceanic radiocarbon: Separation of the natural and bomb components, *Global Biogeochem. Cycles*, 9, 263-288, 1995.

Brzezinski, M. A., The Si:C:N ratio of marine diatoms: Interspecific variability and the effect of some environmental variables, *J. Phycology*, 21, 347-357, 1985.

Charles, C. D., P. N. Froelich, M. A. Zibello, R. A. Mortlock, and J. J. Morley, Biogenic opal in Southern Ocean sediments over the last 450,000 years: Implications for surface water chemistry and circulation, *Paleoceanography*, 6, 697-728, 1991.

Chipman, D. W., J. Marra, and T. Takahashi, Primary production at 47°N and 20°W in the North Atlantic Ocean: A comparison between the ^{14}C incubation method and the mixed layer carbon budget, *Deep Sea Res.*, Part II, 40, 151-169, 1993.

Crowley, T. J., Calcium-carbonate preservation patterns in the central North Atlantic during the last 150,000 years, *Mar. Geol.*, 51, 1-14, 1983.

Crowley, T. J., Late quaternary carbonate changes in the North/Atlantic and Atlantic/Pacific comparisons, in The Carbon Cycle and Atmospheric CO_2: Natural Variations Archean to Present, Geophys. Monogr. Ser., vol. 32, edited by E. T. Sundquist and W. S. Broecker, pp. 271-284, AGU, Washington, D.C., 1985.

Culberson, C. H., and R. M. Pytkowicz, Effect of pressure on carbonic acid, boric acid and the pH in sea water, *Limnol. Oceanogr.*, 13, 403-417, 1968.

Delaney, M. L., and E. A. Boyle, Tertiary paleoceanic chemical variability: Unintended consequences of simple geochemical models, *Paleoceanography*, 3, 137-156, 1988.

DeMaster, D. J., The supply and accumulation of silica in the marine environment, *Geochim. Cosmochim. Acta*, 45, 1715-1732, 1981.

Dickson, A. G., and J. P. Riley, The estimation of acid dissociation constants in seawater media from potentiometric titrations with strong base, I, The ionic product of water - K_w, *Mar. Chem.*, 7, 89-99, 1979.

Duplessy, J.-C., L. D. Labeyrie, A. Juillet-Leclerc, F. Maitre, J. Dupart, and M. Sarnthein, Surface salinity reconstruction of the North Atlantic Ocean during the last glacial maximum, *Oceanol. Acta*, 14, 311-324, 1991.

Duplessy, J.-C., L. D. Labeyrie, M. Paterne, S. Hovine, T. Fichefet, J. Duprat, and M. Labracherie, High latitude deep water sources during the last glacial maximum and the intensity of the global ocean circulation, in The South Atlantic: Present and Past Circulation, edited by G. Wefer et al., pp. 445-460, Springer-Verlag, New York, 1996.

Dymond, J., and M. Lyle, Flux comparisons between sediments and sediment traps in the eastern tropical Pacific: Implications for CO_2 variation during the Pleistocene, *Limnol. Oceanogr.*, 30, 699-712, 1985.

Edmond, J. M., and J. M. T. M. Gieskes, On the calculation of the degree of saturation of sea water with respect to calcium carbonate under in situ conditions, *Geochim. Cosmochim. Acta*, 34, 1261-1291, 1970.

Eppley, R. W., and B. J. Peterson, Particulate organic matter flux and planktonic new production in the deep ocean, *Nature*, 282, 677-680, 1979.

Farrell, J. W., and W. L. Prell, Climatic change and $CaCO_3$ preservation: An 800,000 year bathymetric reconstruction from the central equatorial Pacific Ocean, *Paleoceanography*, 4, 447-466, 1989.

Farrell, J. W., and W. L. Prell, Pacific $CaCO_3$ preservation and $\delta^{18}O$ since 4 Ma: Paleoceanic and paleoclimatic implications, *Paleoceanography*, 6, 485-498, 1991.

Friedli, H., H. Loetscher, H. Oeschger, U. Siegenthaler, and B. Stauffer, Ice core record of the $^{13}C/^{12}C$ record of atmospheric CO_2 in the past two centuries, *Nature*, 324, 237-238, 1986.

Froelich, P. N., V. Blanc, R. A. Mortlock, S. N. Chillrud, W. Dunstan, A. Udomkit, and T.-H. Peng, River fluxes of dissolved silica to the ocean were higher during glacials: Ge/Si in diatoms, rivers, and oceans, *Paleoceanography*, 7, 739-767, 1992.

Hales, B., and S. Emerson, Calcite dissolution in sediments of the Ontong-Java Plateau: In situ measurements of pore water O_2 and pH, *Global Biogeochem. Cycles*, 10, 527-541, 1996.

Heinze, C., Zur Erniedrigung des atmosphärischen Kohlendioxidgehalts durch den Weltozean während der letzten Eiszeit, Ph.D. thesis, Max-Planck-Inst. für Meteorol., 180 pp., Hamburg, Germany, 1990.

Heinze, C., and T. J. Crowley, Sedimentary response to ocean gateway circulation changes, *Paleoceanography*, 12, 742-754, 1997.

Heinze, C., and E. Maier-Reimer, The Hamburg Oceanic Carbon Cycle Circulation Model, Deutsch. Klimarechenzentrum, Tech. Rep. 5, 32 pp., Hamburg, Germany, 1992.

Heinze, C., E. Maier-Reimer, and K. Winn, Glacial pCO_2 reduction by the world ocean: Experiments with the Hamburg carbon cycle model, *Paleoceanography*, 6, 395-430, 1991.

Heinze, C., P. Schlosser, and E. Maier-Reimer, Transient tracers in a global OGCM: Source functions and simulated distributions, *J. Geophys. Res.*, 103(C8), 15,903-15,922, 1998.

Hellerman, S., and M. Rosenstein, Normal monthly wind stress over the world ocean with error estimates, *J. Phys. Oceanogr.*, 13, 1093-1104, 1983.

Herguera, J. C., Deep-sea benthic foraminifera and biogenic opal: Glacial to postglacial productivity changes in the Western Equatorial Pacific, *Mar. Micropaleontol.*, 19, 79-98, 1992.

Honjo, S., S. J. Manganini, and J. J. Cole, Sedimentation of biogenic matter in the deep ocean, *Deep Sea Res.*, Part A, 29, 609-625, 1982.

Hurd, D. C., Factors affecting solution rate of biogenic opal in seawater, *Earth Planet. Sci. Lett.*, 15, 411-417, 1972.

Hurd, D. C., Interactions of biogenic opal, sediment and seawater in the Central Equatorial Pacific, *Geochim. Cosmochim. Acta*, 37, 2257-2282, 1973.

Jahnke, R. A., The global cean flux of particulate organic carbon: Areal distribution and magnitude, *Global Biogeochem. Cycles*, 10, 71-88, 1996.

Keir, R. S., The dissolution kinetics of biogenic calcium carbonates in seawater, *Geochim. Cosmochim. Acta*, 44, 241-252, 1980.

Keller, G., and J. A. Barron, Paleoceanographic implications of Miocene deep-sea hiatuses, *Geol. Soc. Am. Bull.*, 94, 590-613, 1983.

Kumar, N., R. F. Anderson, R. A. Mortlock, P. N. Froelich, P. Kubik, B. Dittrich-Hannen, and M. Suter, Increased biological productivity and export production in the glacial Southern Ocean, *Nature*, 378, 675-680, 1995.

Lasaga, A. C., R. A. Berner, and R. M. Garrels, An improved geochemical model of atmospheric CO_2 fluctuations over the past 100 million years, in The Carbon Cycle and Atmospheric CO_2: Natural Variations Archean to Present, Geophys. Monogr. Ser., vol. 32, edited by E. T. Sundquist and W. S. Broecker, pp. 397-411, AGU, Washington, D.C., 1985.

Leinen, M., D. Cwienk, G. R. Heath, P. E. Biscaye, V. Kolla, J. Thiede, and J. P. Dauphin, Distribution of biogenic silica and quartz in recent deep-sea sediments, *Geology*, 14, 199-203, 1986.

Levitus, S., Climatological atlas of the world ocean, Prof. Pap. 13, Natl. Oceanic and Atmos. Admin., U.S. Dept. of Commer., Washington, D.C., 1982.

Li, Y.-H., and S. Gregory, Diffusion of ions in sea water and in deep-sea sediments, *Geochim. Cosmochim. Acta*, 38, 703-714, 1974.

Lisitsyn, A. P., Basic relationships in distribution of modern siliceous sediments and their connection with climatic zonation, 1, *Int. Geol. Rev.*, 9(5), 631-652, 1986a.

Lisitsyn, A. P., Basic relationships in distribution of modern siliceous sediments and their connection with climatic zonation, 2, *Int. Geol. Rev.*, 9(6), 842-865, 1986b.

Lisitsyn, A. P., Basic relationships in distribution of modern siliceous sediments and their connection with climatic zonation, 3, *Int. Geol. Rev.*, 9(8), 1114-1130, 1986c.

Lisitzin, A. P., Distribution of siliceous microfossils in suspension and bottom sediments, in The Micropaleontology of Oceans, edited by B. M. Funnell and W. R. Reidel, pp. 173- 195, Cambridge Univ. Press, New York, 1971.

Lorenz, S., B. Grieger, P. Helbig, and K. Herterich, Investigating the sensitivity of the Atmospheric General Circulation Model ECHAM 3 to paleoclimatic boundary conditions, *Geol. Rundsch.*, 85, 513-524, 1996.

Lyle, M., D. W. Murray, B. P. Finney, J. Dymond, J. M. Robbins, and K. Brooksforce, The record of late pleistocene biogenic sedimentation in the Eastern Tropical Pacific Ocean, *Paleoceanography*, 3, 39-59, 1988.

Maier-Reimer, E., On the effect of sediments on the airborne fraction, in Proceedings of the Third International Conference on Analysis and Evaluation of Atmospheric CO_2 data present and Past, Hinterzarten, 16-20 October 1989, Rep. 59, pp. 217-220, Environ. Pollut. Monit. and Res. Programme, World Meteorol. Organ., Geneva, 1989.

Maier-Reimer, E., Geochemical cycles in an ocean general circulation model. Pre-industrial Tracer Distributions, *Global Biogeochem. Cycles*, 7, 645-677, 1993.

Maier-Reimer, E., and R. B. Bacastow, Modelling of geochemical tracers in the ocean, in Climate-Ocean Interaction, edited by M. E. Schlesinger, pp. 233-267, Kluwer Acad., Norwell, Mass., 1990.

Maier-Reimer, E., and K. Hasselmann, Transport and storage of CO_2 in the ocean - an inorganic ocean-circulation carbon cycle model, *Clim. Dyn.*, 2, 63-90, 1987.

Maier-Reimer, E., U. Mikolajewicz, and K. Hasselmann, Mean circulation of the Hamburg LSG OGCM and its sensitivity to the thermohaline surface forcing, *J. Phys. Oceanogr.*, 23, 731-757, 1993.

Martin, J. H., G. A. Knauer, D. M. Karl, and W. W. Broenkow, VERTEX: Carbon cycling in the northeast Pacific, *Deep Sea Res.*, Part A, 34, 267-285, 1987.

Mikolajewicz, U., E. Maier-Reimer, T. J. Crowley, and K.-Y. Kim, Effect of Drake and Panamanian gateways on the circulation of an ocean model, *Paleoceanography*, 8, 409-426, 1993.

Mortlock, R. A., C. D. Charles, P. N. Froelich, M. A. Zibello, J. Saltzman, J. D. Hays, and L. H. Burckle, Evidence for lower productivity in the Antarctic Ocean during the last glaciation, *Nature*, 351, 220-223, 1991.

Munhoven, G., and L. M. François, Glacial-interglacial variability of atmospheric CO_2 due to changing continental silicate rock weathering: A model study, *J. Geophys. Res.*, 101, 21,423-21,437, 1996.

Najjar, R. G., J. L. Sarmiento, and J. R. Toggweiler, Downward transport and fate of organic matter in the ocean: Simulations with a general circulation model, *Global Biogeochem. Cycles*, 6, 45-76, 1992.

Neftel, A., E. Moor, H. Oeschger, and B. Stauffer, Evidence from polar ice cores for the increase in atmospheric CO_2 in the past two centuries, *Nature*, 315, 45-47, 1985.

Nelson, D. M., P. Tréguer, M. A. Brzezinski, A. Leynaert, and B. Quéguiner, Production and dissolution of biogenic silica in the ocean: Revised global estimates, comparison with regional data and relationship with biogenic sedimentation, *Global Biogeochem. Cycles*, 9, 359-372, 1995.

Packard, T. T., M. Denis, M. Rodier, and P. Garfield, Deep-ocean metabolic CO_2 production: Calculations from ETS activity, *Deep Sea Res.*, Part A, 35, 371-382, 1988.

Parsons, T. R., and M. Takahashi, Biological Oceanographic Processes, 186 pp., Pergamon, Tarrytown, N.Y., 1973.

Peterson, L. C., and W. L. Prell, Carbonate preservation and rates of climatic change: An 800 kyr record from the Indian Ocean, in The Carbon Cycle and Atmospheric CO_2: Natural Variations Archean to Present, Geophys. Monogr. Ser., vol. 32, edited by E. T. Sundquist and W. S. Broecker, pp. 251-269, AGU, Washington, D.C., 1985.

Ragueneau, O., A. Leynaert, P. Tréguer, D. J. DeMaster, and R. F. Anderson, Opal studied as a marker of paleoproductivity, *EOS trans.*, AGU, 77(49), 491, 493, 1996.

Roy, R. N., L. N. Roy, M. Lawson, K. M. Vogel, C. Porter-Moore, W. Davis, F. J. Millero, and D. M. Campbell, Determination of the ionization constants of carbonic acid in seawater, *Mar. Chem.*, 44, 249-259, 1993.

Sanyal, A., N. G. Hemming, G. N. Hanson, and W. S.

Broecker, Evidence for a higher pH in the glacial ocean from boron isotopes in foraminifera, *Nature*, 373, 234-236, 1995.

Schink, D. R., and N. L. Guinasso Jr., Effects of bioturbation on sediment-seawater interactions, *Mar. Geol.*, 23, 133-154, 1977.

Schink, D. R., and N. L. Guinasso Jr., Redistribution of dissolved and adsorbed materials in abyssal marine sediments undergoing biological stirring, *Am. J. Sci.*, 278, 687-702, 1978.

Shackleton, N. J., and N. G. Pisias, Atmospheric carbon dioxide, orbital forcing, and climate, in The Carbon Cycle and Atmospheric CO_2: Natural Variations Archean to Present, Geophys. Monogr. Ser., vol. 32, edited by E. T. Sundquist and W. S. Broecker, pp. 303-317, AGU, Washington, D.C., 1985.

Six, K., and E. Maier-Reimer, Effects of plankton dynamics on seasonal carbon fluxes in an ocean general circulation model, *Global Biogeochem. Cycles*, 10, 559-583, 1996.

Soetaert, K., P. M. J. Herman, J. J. Middelburg, C. Heip, H. S. deStigter, T. C. E. van Weering, E. Epping, and W. Helder, Modeling ^{210}Pb-derived mixing activity in ocean margin sediments: Diffusive versus nonlocal mixing, *J. Mar. Res.*, 54, 1207-1227, 1996.

Staffelbach, T., B. Stauffer, A. Sigg and H. Oeschger, CO_2 measurements from polar ice cores: More data from different sites, *Tellus*, Ser. B, 43B, 91-96, 1991.

Suess, E., Particulate organic carbon flux in the oceans - Surface productivity and oxygen utilization, *Nature*, 288, 260-263, 1980.

Takahashi, T., W. S. Broecker, and S. Langer, Redfield ratio based on chemical data from isopycnal surfaces, *J. Geophys. Res.*, 90, 6,907-6,924, 1985.

Tréguer, P., D. M. Nelson, A. J. Van Bennekom, D. J. DeMaster, A. Leynaert, and B. Quéguiner, The balance of silica in the world ocean: A re-estimate, *Science*, 268, 375-379, 1995.

Ullman, W. J., and R. C. Aller, Diffusion coefficients in nearshore marine environments, *Limnol. Oceanogr.*, 27, 552-556, 1982.

Van Bennekom, A. J., Silica signals in the South Atlantic, in The South Atlantic: Present and Past Circulation, edited by G. Wefer et al., pp. 345-354, Springer-Verlag, New York, 1996.

Van Bennekom, A. J., A. G. J. Buma, and R. F. Nolting, Dissolved aluminum in the Weddell-Scotia Confluence and the effect of Al on the dissolution kinetics of biogenic silica, *Mar. Chem.*, 35, 423-434, 1991.

Van Bennekom, A. J., J. H. F. Jansen, S. J. van der Gaast, J. M. van Iperen and J. Pieters, Aluminium-rich opal: An intermediate in the preservation of biogenic silica in the Zaïre (Congo) deep-sea fan, *Deep Sea Res.*, Part A, 36, 173-190, 1989.

Van Cappellen, P., and L. Qiu, Biogenic silica dissolution in sediments of the Southern Ocean, I, Solubility, *Deep Sea Res.*, Part II, 44, 1109-1128, 1997a.

Van Cappellen, P., and L. Qiu, Biogenic silica dissolution in sediments of the Southern Ocean, II, Kinetics, *Deep Sea Res.*, Part II, 44, 1129-1149, 1997b.

Vanderborght, J.-P., R. Wollast and G. Billen, Kinetic models of diagenesis in disturbed sediments, 1, Mass transfer properties and silica diagenesis, *Limnol. Oceanogr.*, 22, 787-793, 1977.

Volk, T., and M. Hoffert, Ocean carbon pumps: Analysis of relative strengths and efficiencies in ocean-driven pCO_2 changes, in The Carbon Cycle and Atmospheric CO_2: Natural Variations Archean to Present, Geophys. Monogr. Ser., vol. 32, edited by E. T. Sundquist and W. S. Broecker, pp. 99-110, AGU, Washington, D.C., 1985.

Winguth, A. M. E., Assimilation von δ^{13}C-Daten aus marinen Sedimentbohrkernen in das LSG zur Rekonstruktion der Ozeanzirkulation während des letzten glazialen Maximums, Ph.D. thesis, 149 pp., Fachbereich Geowissenschaften, Univ. Hamburg, Hamburg, Germany, 1997.

Winguth, A. M. E., E. Maier-Reimer, U. Mikolajewicz, and J.-C. Duplessy, On the sensitivity of an ocean general circulation model to glacial boundary conditions, Rep. 203, 48 pp., Max-Planck-Institut für Meteorologie, Hamburg, Germany, 1996.

Woodruff, S. D., R. J. Slutz, R. L. Jenne, and P. M. Steuer, A comprehensive ocean-atmosphere data set, *Bull. Am. Meteorol. Soc.*, 68, 1239-1250, 1987.

D. Archer and A. M. E. Winguth, Department of the Geophysical Sciences, 5734 South Ellis Avenue, University of Chicago, Chicago, IL 60637. (email: d-archer@uchicago.edu; winguth@starbuck.uchicago.edu)

C. Heinze and E. Maier-Reimer, Max-Planck-Institut für Meteorologie, Bundesstrasse 55, D-20146 Hamburg, Germany. (email: heinze@dkrz.de; maier-reimer@dkrz.de)

(Received February 12, 1998; revised July 1, 1998; accepted August 25, 1998.)